Microstructure-sensitive Crystal Viscoplasticity for Ni-base Superalloys Targeting Long-term Creep-Fatigue Interaction Modeling

Year 3 Report

Reporting Period: October 1, 2015 to September 30, 2016

Professor Richard W. Neu

Graduate Research Assistants:
Ernesto Estrada Rodas, Sanam Gorgan Nejad, Anirudh Bhat

George W. Woodruff School of Mechanical Engineering /
School of Materials Science and Engineering
Georgia Institute of Technology
Atlanta, GA 30332

September 30, 2016

U. S. Department of Energy
National Energy Technology Laboratory
University Turbine Systems Research
Award: DE-FE0011722

Topic Area 2 – Hot Gas Path Research and Development

DISCLAIMER

ABSTRACT

The aim of this project is to develop a microstructure-sensitive crystal viscoplasticity (CVP) model for single-crystal Ni-base superalloys to model the behavior of the material and components in the hot gas path sections of industrial gas turbines (IGT). Microstructure degradation associated with aging critical to predicting long-term creep-fatigue interactions will be embedded into the model through the γ' precipitate morphology evolution by coupling the coarsening drivers and kinetics into the constitutive equations of the CVP model. Model parameters will be determined using new experimental protocols that involve systematically artificially aging the alloy under different stress conditions to determine the relationship between the size and morphology γ' precipitates on the creep and thermomechanical fatigue response.

TABLE OF CONTENTS

EXECUTIVE SUMMARY

With increasing hot gas path temperature, more demands are placed on the materials in the hot gas path, requiring designs to employ single crystal Ni-base superalloys in industrial gas turbines (IGT). Completely eliminating grain boundaries improves creep behavior but increase temperatures also increases thermal transients. Currently, "short" duration (<3000 cycles (TMF), <30,000 hrs (Creep)) laboratory tests are used to predict component lifetimes designed to be greater than these cycles and times. A critical limitation of current remaining life prediction models is that they do not explicitly account for the changes in the microstructural degradation occurring under high temperature exposure over long-term service conditions typical of IGT. Therefore, consideration of microstructural degradation is key to developing more robust creep-fatigue life models for these hot section alloys to extend predictions outside the typical laboratory test regime. Another critical limitation of current remaining life prediction models is that they do not explicitly account for the duty cycle such as peakers or baseload operation of IGT and understanding the microstructural changes during usage will also be key to predict the residual life of the components.

The understanding of the effects of aged microstructures on the thermomechanical properties of Ni-base superalloys remains unclear. Of the few experimental results available in this area, the results are mixed, some promote aged microstructures as beneficial, while others as detrimental. The importance of these aged structures arises from the fact that when components used in the hot sections of IGT engines remain in service for extended periods of time, the local temperature and stress provides the catalyst for the evolution of the microstructure. Further, in the design of components that comprise the hot sections of IGTs, designers use material models assuming the mechanical properties are that of the as-cast and heat-treated material even for simulations of years of the component usage.

To account for these extreme hot section environments employing highly anisotropic single-crystal alloys, a physics-based temperature-dependent, microstructure-sensitive life analysis tool based on crystal viscoplasticity (CVP) is being developed that captures

i. the crystal orientation which controls both elastic and inelastic anisotropy,
ii. the temperature dependence on the mechanism of the creep deformation and its interaction with microstructure and low-temperature fatigue deformation mechanism,
iii. complex cyclic thermomechanical boundary conditions leading to extreme local thermal gradients,
iv. the influence of the evolution of microstructure (e.g., coarsening and rafting of the γ') with long-term exposure to elevated temperature under sustained stress through internal state variables without explicitly modeling the γ' precipitates and γ matrix, and
v. the influence of the evolution of microstructure near exposed surfaces due to environmental considerations such as oxidation and embrittlement.

Constitutive models available in commercial finite element codes used to address creep-fatigue interactions in single crystal Ni-base superalloys are limited to non-interaction creep and plasticity models which cannot address the physical processes or microstructural evolution. An enhanced CVP model is needed that has broad utility in the design and maintenance of hot section materials

and components of IGT when conventional isotropic creep-fatigue constitutive models are not applicable. The CVP enables the engineer to predict component response using thermomechanical boundary conditions, to understand the influence of thermal transients associated with efficient and effective cooling strategies as well as load-cycle gas turbines, to perform component analysis investigating the interaction between geometric discontinuities and crystal orientation of the material, to determine the crack tip stress fields for predicting creep-fatigue crack growth, and to study role of defects such as freckles important for process and materials design.

This report summarizes work performed in Year 3 including aging studies conducted on single crystal Ni-base superalloy CMSX-8, and the development of the microstructure-sensitive CVP model for CMSX-8 including its calibration from creep-fatigue experiments and its implementation in analysis codes. The details of this work are described in two documents recently prepared: "Aging Kinetics of Ni-base Superalloys" (Appendix 1) and "On the Development of ICME Tools for Creep and Aging of CMSX-8" (Appendix 2).

APPENDIX 1

Aging kinetics of Ni-base superalloys

Sanam Gorgannejad [a], Ernesto A. Estrada Rodas[a], Richard W. Neu[a,b]

[a]*The George W. Woodruff School of Mechanical Engineering, Georgia Institute of Technology, Atlanta, GA, USA*

[b]*School of Materials Science and Engineering, Georgia Institute of Technology, Atlanta, GA, USA*

ABSTRACT

In the present work, the degradation of the γ/γ' microstructure of single crystal Ni-base superalloy, CMSX-8, has been studied experimentally and computationally. Two microstructure evolution processes, referred to as rafting and coarsening, have been decoupled and investigated independently. The kinetics of coarsening and rafting of γ' precipitates have been characterized using scanning electron microscopy for specimens at temperatures ranging from 900 °C to 1120 °C and under stress levels of 25 to 360 MPa. A phenomenological relation describing rafting as a function of stress, temperature and time was fitted to experimental data. It was determined that coarsening of γ' precipitates follows the LSW cube rate law and is controlled by a volume diffusion mechanism. The effective diffusivity which influences the aging behavior was estimated computationally using DICTRA software and the coarsening experimental results were verified by formulating and computing the effective activation energy in multicomponent systems.

Keywords: Ni-base superalloys, CMSX-8, rafting, coarsening, activation energy, DICTRA

1. INTRODUCTION

Nickel-base superalloys owing to their remarkable high temperature strength and stability have been widely used in the hot path of turbine engines. The superior properties are attributed to the precipitate hardened structure by ordered $L1_2$ phase with FCC structure distributed by heat treatment in disordered γ phase. Modified second-generation single-crystal Ni-base superalloy CMSX-8, has been developed by the Cannon-Muskegon Corporation [1] with similar composition as CMSX-4, but with the content of the high cost rare element Re reduced by one half. The severe service conditions result in substantial degradation of the microstructure that ultimately alters the response of the material. Therefore, it is of great importance to investigate the kinetics of microstructural evolution.

Under the combined influence of stress and high temperature, the γ' precipitates degrade to a plate-like morphology, the direction of which is controlled by the lattice misfit parameter [2],

$$\delta = \frac{2\left(a_{\gamma'} - a_{\gamma}\right)}{a_{\gamma'} + a_{\gamma}} \qquad (1)$$

where a_{γ} and $a_{\gamma'}$ are the lattice parameters of γ and γ' phases, respectively. Most modern Ni-base superalloys are classified as negative misfit alloys which form rafts normal to the loading direction under tensile stress, so called N-type rafts [2, 3].

The rafting process includes two sequential regimes with distinct mechanisms; these two are often referred to as "elastic" and "plastic" regimes of rafting. The driving force for rafting in the elastic regime is the elastic strain energy difference between the horizontal and vertical γ channels [2, 4]. The onset of rafting in the elastic regime takes place at very low stresses. The morphology of precipitates remains cuboidal and the coherency of the γ/γ' interface is retained. Therefore, once the applied load is removed, the strain energy gradient is eliminated and the rafting process is inhibited. However, in the plastic regime of rafting, once the dislocation networks are formed and the coherency of the interfaces is lost, rafting will proceed even in the absence of applied load [4]. The transition from elastic to plastic regime is determined by a plastic strain threshold of 0.1 % ± 0.03%, below which kinetics of rafting is immeasurably slow [4]. In general, if the plastic regime of rafting is active, rafting in the elastic regime can be neglected due to small morphological changes and slow rates. In this study, the kinetics of microstructural evolution as a result of rafting in the plastic regime has been characterized. Apart from the rafting process, coarsening of γ' precipitates is an active process during and subsequent to rafting. The coherent precipitates are subjected to coarsening while rafting is occurring and once the microstructure evolves to the fully rafted state, coarsening becomes the dominant process. In the present paper, coarsening and rafting processes that take place simultaneously have been decoupled. A reliable study that provides an accurate prediction

of the microstructure state at different service conditions requires considering the contribution of both processes and characterizing the kinetics of each independently. The classic theory of LSW developed by Lifshitz, Slyozov [5] and Wagner [6] is used to describe the coarsening of precipitates according to cubic rate law,

$$r^3 - r_0^3 = kt \qquad (2)$$

Such a process is called Ostwald ripening after a chemist who initially described the process qualitatively [7].

The coarsening rate constant, k, is given by

$$k = \frac{8C_e D_{eff} \sigma \Omega^2}{9RT} \qquad (3)$$

where C_e is the total equilibrium mole fraction of solute in the matrix, D_{eff} is the effective diffusion coefficient of the γ matrix, σ is the precipitate/matrix interfacial energy, Ω is the molar volume of the precipitate, R is the gas constant and T is the absolute temperature. In the present study after characterizing the kinetics of microstructure degradation in CMSX-8, the effective diffusivity in the γ channels that controls the aging behavior is estimated by employing DICTRA software [8]. DICTRA is designed to simulate diffusion-controlled transformations and in this study it is used to evaluate the effective activation energy during coarsening to verify the results acquired from aging experiments.

2. EXPERIMENTAL PROCEDURE

2.1 Material description and experimental methods

CMSX-8 is a modification of a second generation single crystal Ni-base superalloy, CMSX-4, with reduced Re content. The nominal composition of these alloys are shown in Table 1. Single crystal bars oriented in [001] direction, were cast by PCC Airfoils in the form of 15.9 mm diameter rods and then solution and double age treated, using proprietary conditions typical for blade components to achieve the initial γ/γ' microstructure. Heat treatment creates cuboidal primary γ' precipitates and fine secondary γ', dispersed in the γ matrix. Considering the rapid disappearance of secondary γ' precipitates under the aging conditions, the size and morphology evolution of the primary precipitates will be our focus in the present study.

Table 1 Chemical compositions (wt. %).

Element	CMSX-8	CMSX-4
Cr	5.4	6.5
Co	10.0	9.6
Mo	0.6	0.6
W	8.0	6.4
Al	5.7	5.6
Ti	0.7	1.0
Ta	8.0	6.5
Re	1.5	3.0
Hf	0.2	0.1
Ni	Bal	Bal

The micrograph of Figure 1 illustrates the typical two phase solution heat treated microstructure composed of γ' cubic precipitates distributed uniformly in γ channels with the volume fraction of 0.7±0.03. The size of the γ channels and γ' precipitates were measured to be about 0.14 μm and 0.74 μm, respectively. These measurements were done using n-point correlation statistics presented in the following section of this work. The cubic shape of the precipitates is attributed to the γ/γ' lattice mismatch and elastic strains which is detailed elsewhere [2]. The dendritic structure is also observed by optical microscope in Figure 2. The MC and $M_{23}C_6$ type carbides are formed in the interdendritic regions and they exhibit blocky and Chinese script morphologies.The primary and secondary dendrite arm spacing mean sizes of 644±150 μm and 112±37 μm, were measured respectively using optical microscope images.

To investigate the kinetics of stress-assisted microstructure degradation (rafting) as a function of applied stress and temperature, a novel and efficient experimental technique was introduced. As is illustrated in Figure 3, specimens with tapered geometry and circular cross section were designed to create linear stress gradient along the sample. The cross section diameter varies from 12.7 mm to 6.35 mm within a 50.8 mm length. Hence, an applied stress distribution that varies by a factor of four between the largest and smallest cross-section of the specimen is achieved. This method reduces the number of required tests by providing the means to characterize the microstructure evolution in a broad

range of stress levels in a single specimen. Constant axial force was applied on specimens at elevated temperatures ranging from 900 °C to 1120°C for different dwell times. Details of the degradation conditions are listed in Table 2.

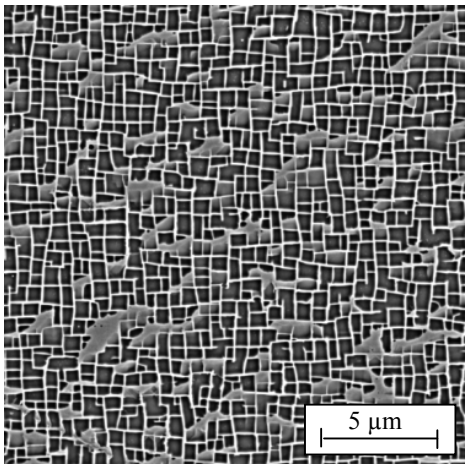

Figure 1 SEM image of CMSX-8 microstructure in the primary dendrite region.

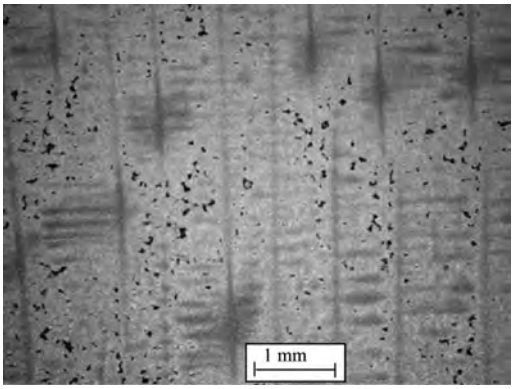

Figure 2 Optical image of the dendritic structure of CMSX-8.

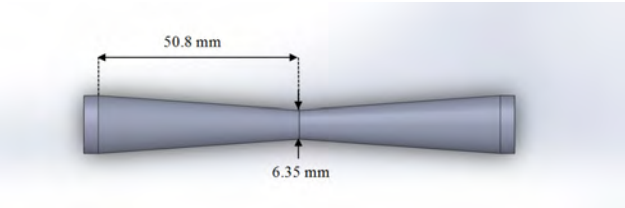

Figure 3 Tapered geometry generating a stress gradient along the specimen.

In order to study the stress-free aging behavior, single-crystal rods were sectioned into small pieces of 0.25 inch in height and were subjected to temperatures of 900 °C, 950 °C and 1100 °C for different exposure times ranging from 25 to 940 hours. Specimens underwent the standard metallographic procedure and subsequent etching by the PW#17 etchant, composed of 100 ml HNO_3, 100 ml HCl, 100 ml H_2O and 3g $MoO_3.H_2O$. Image quantification was carried out using SEM micrographs and the n-point correlation method which is described in the next section.

Table 2 Degradation conditions for stress-assisted aging tests.

Temperature [°C]	Stress [MPa] (min, max)	Dwell time [h]
900	(90,360)	320
950	(40,150)	445
1120	(25,100)	50

2.2 Image quantification using the 2-point statistics method

Microstructures are better quantified using statistical measurements of their morphology. In the case of CMSX-8, metrics like precipitate size, channel width and volume fraction will generally follow statistical distributions that can be represented by the use of n-point statistics. With n-point statistics, a mathematical representation of the microstructure can be obtained from a micrograph in which a probability density function is used to predict the likelihood of a material phase being present at each pixel in the image. This makes n-point statistics particularly powerful in characterizing the spatial arrangement and anisotropy of microstructural attributes [9, 10]. The initial proposal of n-point statistics was mathematically rigorous and involved the solution of complicated convolution integrals; however, Fullwood et al.[11] have shown that spectral techniques can be used to rapidly evaluate these equations on a 2-phase composite, significantly reducing the complexity of the calculation. This is achieved by discretizing the microstructure and assigning a material phase to each pixel in the image. CMSX-8 can be considered a 2-phase composite where the γ' precipitates are one phase and the γ channels are the other; thus a 2-point statistics approach would be sufficient to mathematically describe its microstructure.

SEM micrographs of CMSX-8 were converted to black and white binary images allowing for a clear distinction between each material phase as shown in Figure 4.

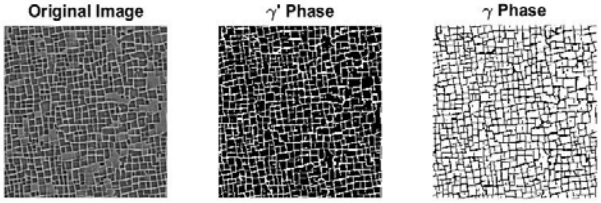

Figure 4 Digitalization of the microstructure.

This procedure enables digitizing the microstructure such that only one material phase is assigned to each pixel. Next, a microstructure function $m(\boldsymbol{x}, n)$ is defined as done by Fullwood et al. [11]. This function indicates the probability of finding a distinct material phase, *n*, at position $\boldsymbol{x}$ in the micrograph. The 1-point correlation function is used to calculate the volume fraction of constituent *n* and is given in its discretized form as [12],

$$f^n = \frac{1}{S}\sum_{s=0}^{s-1} m_s^n \qquad (4)$$

where *S* denotes the number of pixels or grid points of the binary image. The 2-point correlation function is defined by [9],

$$f\left(n,n' \mid \boldsymbol{r}\right) = \frac{1}{vol\left(\Omega \mid \boldsymbol{r}\right)} \iiint_{x\in\Omega \mid \boldsymbol{r}} m\left(\boldsymbol{x},n\right) m\left(\boldsymbol{x}+\boldsymbol{r},n'\right) d\boldsymbol{x} \qquad (5)$$

where $f(n,n' \mid \boldsymbol{r})$ represents the probability density function of finding a material phase *n* and *n'* at two ordered points separated by a vector $\mathbf{r}$. Because the calculation is performed in the domain $\boldsymbol{\Omega}$, which is the microstructure area of interest in the micrograph, the 2-point statistics method analyzes the whole volume of data available in the micrograph, whereas a line measurement done with available optics packages can only sample 2 data points at a time. This makes the method very appealing to obtain statistically representative measurements of microstructural features. For computational implementation, the 2-point correlation function is discretized as,

$$f_t^{nn'} = \frac{1}{S}\sum_{s=0}^{s-1} m_s^n m_{s+t}^{n'} \qquad (6)$$

where *n* and *n'* are the two distinct phases of the material. A special case of correlation is the case when $n \neq n'$; this is called cross-correlation. For a two phase material the correlation and cross-correlation functions have been shown to be the inverse of each other [13]. The correlation and cross-correlation functions are converted to the Fourier domain which allows very rapid evaluation of the 2-point statistics. In our analysis, the center of the *x*-*y* coordinate system is made coincident with the center of the image under consideration. Furthermore, care is taken such that the cubic directions of the crystal, [001] and [010], are aligned with the *x* and *y* direction respectively in the binary images. Then, the probability from the cross-correlation function along either *x* or *y* can be evaluated to measure channel width and precipitate size [14]. The information from the cross-correlation function can then be used to get a statistical measurement of the γ' precipitates and the γ channel width. In Figure 5, both the cross-correlation function and the probability along the *x* and the *y* axis are plotted. In the latter plot, the humps in probability are points where a vector along *x* or *y* started at a γ' precipitate and ended at a γ channel. Because of the symmetry of the microstructure and the symmetric boundary conditions used in the Fourier analysis, the distance from the origin to the first hump in

probability represents the statistical measurement of half of the precipitate size. Similarly, the distance between the first maximum and the first minimum is the statistical measurement of the channel width in this microstructure.

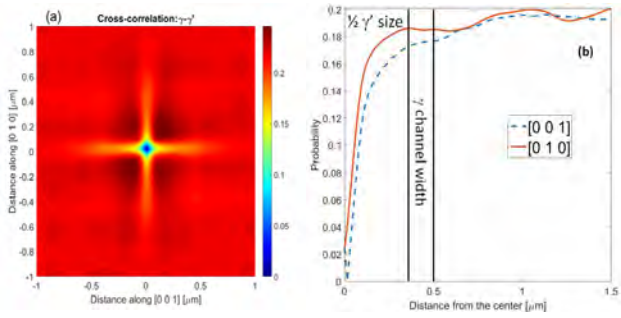

Figure 5 Left: color map of the cross-correlation function. Right: values of the cross-correlation function along *x* and *y* direction

The extent of rafting can be quantified in several manners. Ignat et al. [15] suggested representing the microstructure state by total surface area of γ/γ' interface in horizontal and vertical channels. They introduced dimensionless parameters (R_1^t, R_1^c and R_2) to compare the surface area of precipitate faces parallel and normal to the stress, under different conditions of tensile, compressive and mixed loading. Later, Matan et al. [4] employed the parameter R_1^t and described N-type rafts developed in CMSX-4 single crystals. The R value for unrafted microstructure is equal to 0.5 and it increases by the formation of N-type rafts. However, R parameter had deficiency to indicate the size of γ' precipitates and only morphology evolution was described. Therefore, it was not able to characterize coarsened microstructure under stress-free conditions. Kirka [14] defined two other dimensionless parameters (η and ζ) based on the ratio of γ channel width of rafted microstructure to the unrafted one which allowed to characterize the size and morphology of the microstructures undergoing both rafting and coarsening processes.Tinga et al. [16] developed a relation that describes the state of microstructure under multiaxial loading condition by the rate of precipitate size evolution. This work was based on the study conducted by Epishin et al. [17] in which widening rate of γ channel width indicates the extent of rafting. Tinga et al. [16] made a use of constant γ' volume fraction assumption and microstructure periodicity which is defined as the sum of channel width and precipitate size in three orthogonal directions ($\lambda = h_i + L_i$) to relate the sizes of these two microstructural features.

In the present paper, the kinetics of rafting is evaluated by measuring the horizontal γ channel widening rate since this microstructure feature, unlike the γ' precipitates, is not subjected to coalescence or linkage and measurement of its width can be performed even in the entirely evolved and inversed microstructures. Furthermore, the similar methodology has been employed by other researchers [17, 18] to capture the extent of rafting in CMSX-4. However, during stress-free coarsening, the precipitate size represents the degree of microstructural evolution. Therefore, employing a robust and reliable quantification method such as 2-point correlation is essential for an accurate and repeatable study on microstructure evolution. In addition, the γ' volume fraction of the as-heat-treated and aged specimens were measured using equation (4) and compared against values calculated using computational tools for better understanding of the aging effects on material.

3. KINETICS OF MICROSTRUCTURE DEGRADATION

3.1 Stress-assisted coarsening (rafting)

The microstructure evolution of CMSX-8 under different tensile stresses and temperatures is depicted in Figure 6. As one would expect from a negative lattice misfit superalloy under tensile stress, elongation of the precipitates has occurred normal to the loading direction and a rafted microstructure is clearly observed. The micrographs in Figure 6 (a) and (b) show development of rafts under 35 MPa at 950 °C and 1120 °C, respectively. The microstructure of Figure 6 (a) is at the early stages of rafting where no detectable evolution in precipitate morphology is observed and the cuboidal shape is retained. However, elevated temperature of 1120 °C , dwell time of 50 hours and an equivalent stress level has caused the formation of the microstructure with nearly fully rafted precipitates. Vertical channels have narrowed and been eliminated partly, while widening of the horizontal channels is apparent. As the stress level is increased to 100 MPa in Figure 6 (c) and (d), the previous observation is more noticeable. The formation of rafts is initiated at 950 °C and precipitates have elongated normal to loading direction while at 1120 °C vertical channels have all been removed and the horizontal channel width experienced a 250% increase to 0.5 μm and a fully rafted microstructure is reached. It can be concluded that temperature has a more pronounced effect on rafting than stress, such that the microstructure with a stress level of 100 MPa at 950 °C has not formed the elongated precipitates similar to the ones observed at 1120°C for the lower stress level of 35 MPa. The fact that rafting is a thermally activated diffusion-controlled process justifies the accelerated formation of rafts at higher temperatures.

The volume fraction of γ' precipitates remains constant as the morphology is changing [2, 16, 17]. This implies that elongation of the precipitate in the horizontal direction is associated with its shrinkage in the vertical direction and, therefore, widening of the γ channels is geometrically imposed as well. It is observed in Figure 6 that shrinkage of the vertical channels, which is compensated by the horizontal channel widening, proceeds until they have disappeared completely and the microstructure reaches the fully rafted state (Figure 6 (d)). Extensive rafting and formation of links between precipitates will eventually lead to the inversion of γ/γ' microstructure such that the discontinued disordered γ phase is distributed in the ordered γ' matrix phase which substantially affects the activity of the dislocations [3].

As was discussed earlier, one way to represent the kinetics of microstructure evolution by rafting is through characterization of the horizontal γ channel widening rate. Experimental results were fitted to a phenomenological Arrhenius type relation to assess the thermal and stress induced process. This model has been postulated for rafting in CMSX-4 [17] and it is expected to describe the rafting kinetics of CMSX-8 as well,

$$\dot{w}_{cub}\left(T,\sigma\right) = A exp\left[-\frac{Q - U\left(T\right)\sigma}{RT}\right] \qquad (7)$$

where A is a pre-exponential factor, Q is the rafting activation energy, σ is the applied stress, R is the universal gas constant, T is the absolute temperature and U(T) is the temperature dependent function defined as,

$$U\left(T\right) = U_T\left(T - T_0\right)^n \qquad (8)$$

The exponent n and the factor U_T are the model parameters. The reference temperature T_0 is the temperature below which rafting does not occur. In current study T_0 was chosen to be 850 °C and is close to the reference temperature of CMSX-4 (828 °C) [17].

Figure 7 depicts the increase in channel widening rate versus stress at 900 °C, 950 °C and 1120 °C for CMSX-8 and CMSX-4. The model parameters for CMSX-8 have been obtained by nonlinear regression analysis and are presented in Table 3. The activation energy for rafting is calculated to be 205.8 *kJ/mol*. This activation energy is comparable to CMSX-4 rafting activation energy of 222 *kJ/mol* [17]. The higher activation energy for CMSX-4 is consistent with the higher Re content in this alloy. In addition, by comparing the channel widening rate plots of CMSX-8 to the corresponding ones of CMSX-4, it is noted that CMSX-8 exhibits an accelerated widening rate at all tested temperatures. This observation can also be attributed to the lower Re content in CMSX-8. The refractory element, Re, is known to have a very low diffusion rate in γ matrix due to its large size [19, 20]. The higher Re content of 3% in CMSX-4 compared to 1.5% in CMSX-8 restricts the diffusion of the atoms and higher activation energy is required for diffusing atoms to overcome the barriers.

Figure 7 shows that the accelerated channel widening rate is associated with the increase in stress level. Additionally, there is a significant dependency of the rate of rafting to temperature. However, it is observed that the behavior at 1120 °C deviates from what is predicted by the model. The experimental data points follow the horizontal dashed line at this temperature which represents a saturation level of microstructure evolution as the fully rafted microstructure has been reached. Beyond the saturation level, rafting is decelerated and coarsening becomes the dominant process.

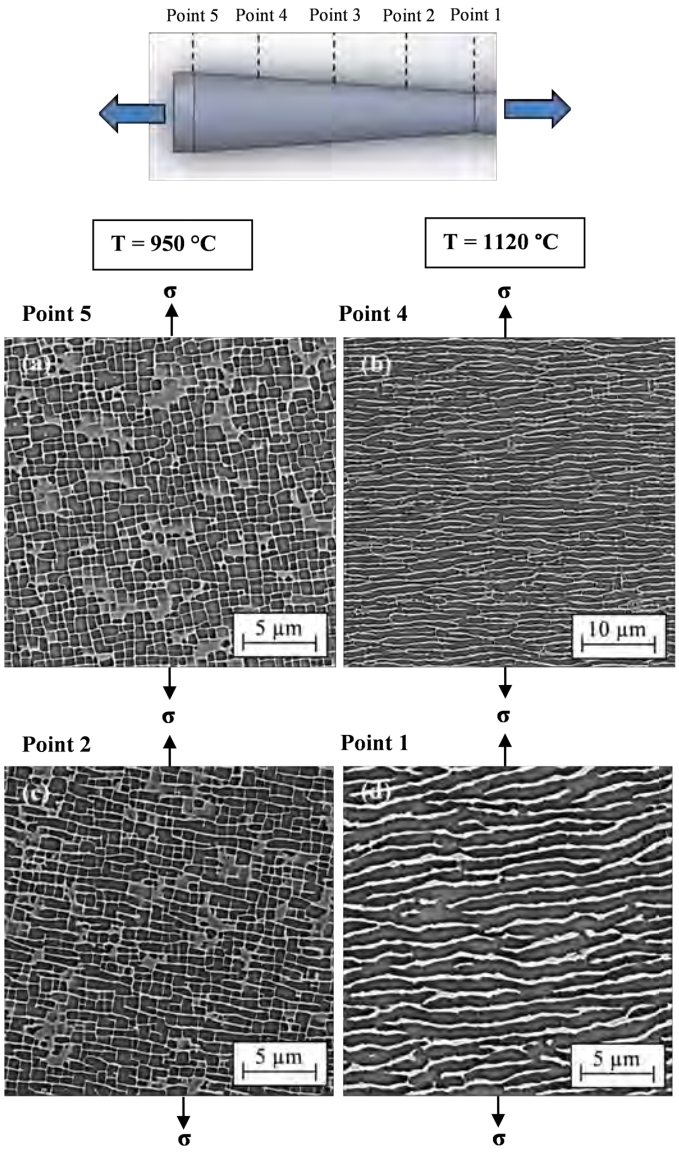

Figure 6 SEM micrographs showing different stages of rafting: (a) 35 MPa, 950 °C, 445 hours (b) 35 MPa, 1120 °C, 50 hours (c) 100 MPa, 950°C, 445 hours (d) 100 MPa, 1120°C, 50 hours.

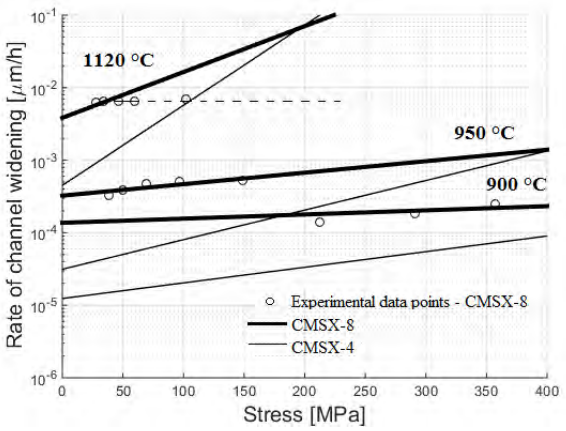

Figure 7 The kinetics of γ channel widening in [001] oriented single crystal, CMSX-8.

Table 3 Rafting kinetics model parameters, CMSX-8.

A [μm/h]	Q [*kJ/mol*]	U_T[J/mol.MPa.K^n]	n
2.0×10^5	205.8	0.033	1.525

By application of external stress along the γ' cube axis, primary slip systems in the γ channels are activated and $a/2\langle 110\rangle\{111\}$ creep dislocations begin to glide in channels. The movement of the dislocations is under the influence of the applied stress and the misfit stresses simultaneously. Under stress-free conditions, in the absence of external stress, the misfit stresses at the γ/γ' horizontal and vertical interfaces are equally distributed. However, the application of external stress will induce a gradient of misfit stresses between the faces of the same precipitate in the vertical and the highly stressed horizontal channels. The influence of the mobile dislocations in γ channels is generally to relieve misfit stresses. Therefore, dislocations subsequently glide from locations with low misfit stress to locations with high misfit stress and are absorbed by the horizontal γ/γ' interfaces. Formation of dislocation networks at the γ/γ' interfaces results in loss of coherency of the γ/γ' interface and relaxation of the misfit stresses in the horizontal channels while the vertical channels are remained coherent [2, 16].

From the outlined mechanism, it is concluded that rafting is a sequential process, initiating from a certain amount of plastic deformation (0.1% for CMSX-4 at 950 °C [4]) in γ channel, and glide of creep dislocation and subsequent loss of coherency. Dislocation networks provide the diffusional path for atoms to travel. The driving force for mass transport is driven by the chemical potential gradient causing the interchange of the neighboring atoms. Therefore, γ partitioning alloying elements such as Cr, Co and Re diffuse to horizontal channels and on the other hand γ' partitioning elements such as Al and Ti travel to vertical channels [21].

As was previously mentioned, the onset of rafting in plastic regime depends on generation and movement of creep dislocations in γ channels. Due to the tapered geometry of the specimens, different levels of creep strain will be introduced. To avoid excessive creep since the focus was on evaluating the alloy in the rafting regime, the stress in the most reduced section was maintained sufficiently low to ensure the occurrence of macroscopic creep strain was minimal. Both the measurement of the initial and final length of the specimens and the measurement of elongation during the test based on a displacement gage outside the furnace suggested that the creep strain accumulated during aging was minimal. Moreover, Serin et al. showed that the rate of γ channel widening is controlled by the maximum principal stress rather than accumulated strain[19].

3.2 Stress-free coarsening

Figure 8 depicts the changes in microstructure that took place during aging at 950 °C for 440 and 940 hours. Comparing to the initial microstructure (Figure 8 (a)), it is evident that the γ' precipitates have increased in size and they tend to become rounded cuboidal shapes. However, the cubic morphology is retained even after 940 hours. This was also observed for temperatures of 900 °C and 1100 °C. Studies conducted on other Ni-base alloys have shown that subsequent to the initial coarsening regime, where the precipitates remain discrete and coherent, the morphology of the particles change to irregular and eventually plate-shaped precipitates, similar to the formation of rafts [22-25]. This is believed to be the consequence of the coalescence of two or more γ' precipitates. Additionally, the elastic interaction of the precipitates induces them to align along crystallographic directions which are soft [26]. This behavior was observed for Rene 88 after 1000 hour at temperatures of 900 °C to 1000 °C [23]. Therefore, the cubic microstructure of CMSX-8 after 940 hours at 950 °C implies the high stability of this material. CMSX-4 with a quite similar composition as CMSX-8 shows the onset of particle coalescence at temperatures higher than 1000 °C and aging times longer than 500 hours [24]. In this study, the microstructure evolution was characterized mainly in the dendritic regions. As was mentioned previously, chemical and particle size inhomogeneity exist between the dendritic and the interdendritic regions, which brings about different lattice misfit values. Accordingly, coherency stresses at γ/γ' interfaces are stronger in dendritic regions and, therefore,

morphology evolution is expected to start earlier in these regions [27]. Consequently, the aging state of the alloy is better characterized by the changes in the microstructure in the dendritic regions.

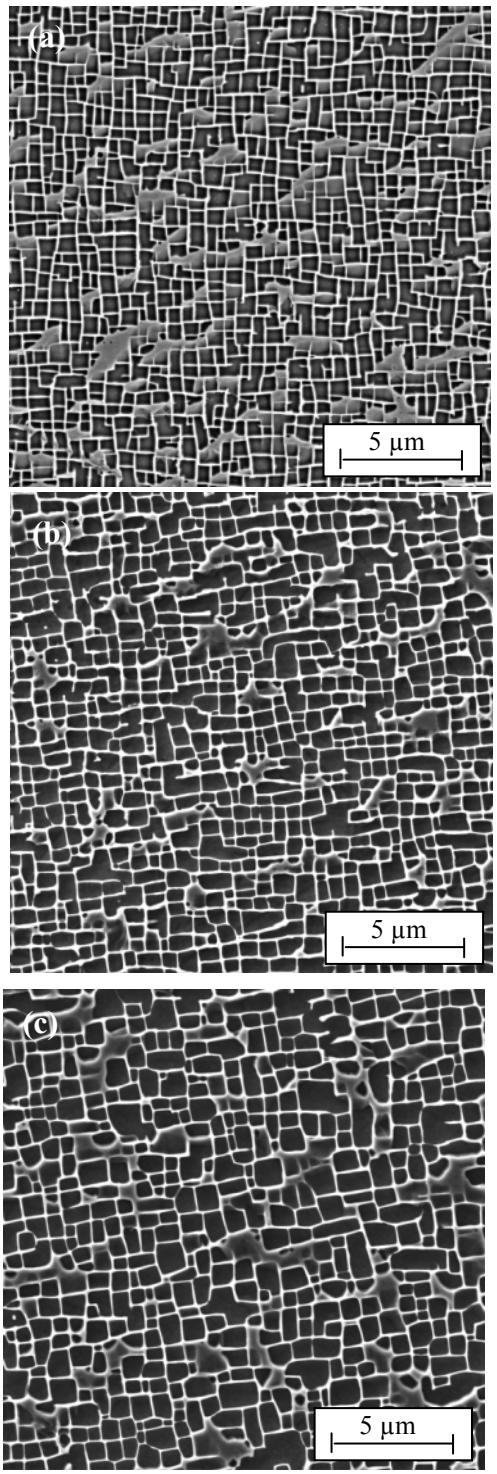

Figure 8 Morphology of γ' precipitates (a) as-heat-treated condition (b) exposed at 950 °C for 440 hours and (c) 940 hours.

The driving force for coarsening was mentioned to be the decrease in interfacial energy. Solute atoms are transported from particles with high curvature to the low curvature ones. In other words, larger particles grow at the expense of smaller ones to dissolve. Thereby, the total

particle number diminishes and the average particle size increases. This competitive growth of particles is known as Ostwald ripening. Coarsening of the γ' precipitates follows the Ostwald ripening phenomena described by the LSW model (equation (2)) suggesting that the volume diffusion is the dominant mechanism for coarsening [22, 24, 28]. The cube rate law assumes that coarsening of a particle is independent of its surroundings, which implies that no elastic interaction exists between particles and their diffusion fields do not overlap [7, 29]. This assumption is limited to alloys with low volume fraction and is not practically applicable to Ni-base superalloys. Despite this issue, as long as the precipitates remain cuboidal and they are not subjected to coalescence, the LSW model may be followed.

The experimental coarsening data yields a good agreement with the LSW cube rate law shown in Figure 9 by the solid lines. Additionally, the relation between $\left(\frac{a}{2}\right)^3$ versus aging time (t) in Figure 10 exhibits a linear trend which implies that the LSW model is capable of capturing the behavior accurately. The mechanism that controls coarsening of discrete and coherent γ' precipitates is volume diffusion or lattice diffusion through which diffusion of atoms occurs by point defects [30].

As was mentioned earlier the microstructure is subjected to morphological evolution to plate-like precipitates at subsequent stages of aging with the driving force of reduction in the interfacial elastic energies by dislocation networks at γ/γ' interface. This behavior can no longer be described by the LSW model in which the elastic interaction of the particles is assumed to be neglected. Eventually, size saturation is reached and the microstructure is stabilized. This stabilization is attributed to the loss of coherency stresses by interfacial dislocations [25]. In order to obtain the size saturated microstructure, long-term aging experiments are required. This was observed for IN939 and Ni-Al-Ta-Mo alloy at 930 °C after 2700 and 1700 hours [23, 25]. Therefore after the early stages of coarsening predicted by the LSW model in Figure 9, the coarsening rate is expected to decelerate and eventually a plateau is reached where the evolved microstructure is stabilized. Conclusively, the LSW model captures the coarsening process that takes place simultaneous to rafting.

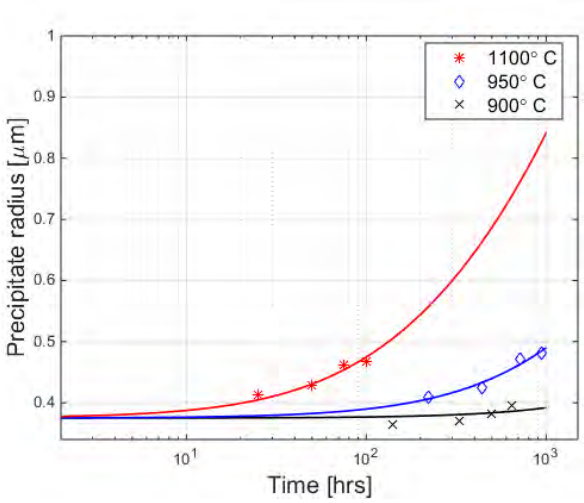

Figure 9 γ' precipitate size evolution with dwell time.

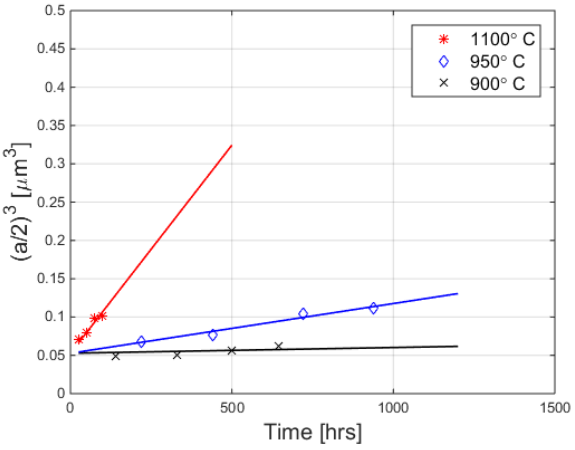

Figure 10 LSW fit to the precipitate size evolution during short-term aging.

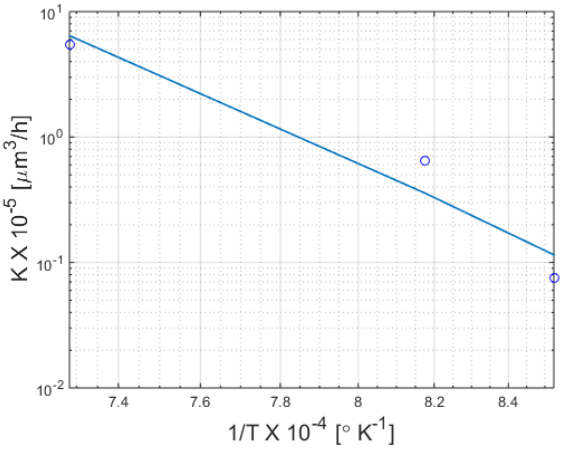

Figure 11 Dependence of the material constant k on the inverse temperature.

The slope of the lines in Figure 10 yields the coarsening rate constant, *k*, at each temperature. Coarsening activation energy can be obtained by plotting ln (*k*) versus 1/T, as shown in Figure 11. The activation energy of 269.4 *kJ/mol* was calculated for CMSX-8, which is approximately equal to CMSX-4 activation energy of 272.4 *kJ/mol* [24]. This value also correlates well to the value of other Ni-base alloys ranging from 247 to 280 *kJ/mol* reported in the literature [22, 24, 29, 31, 32].

The coarsening activation energy obtained by aging experiments can be verified computationally as well. The key is to develop a relation that calculates activation energy as a function of constituents of the system. This composition dependent relation provides the means to evaluate systems of various compositions. The diffusion coefficient term in equation (3) is equivalent to the effective diffusivity of the coarsening process and exhibits an Arrhenius form [24, 33],

$$D_{eff} = D_{0,eff}\, exp\left(-\frac{Q_{eff}}{RT}\right) \tag{9}$$

where Q_{eff} and $D_{0,eff}$ are the activation energy and pre-exponential factor of the effective diffusivity that can be described by arithmetic and harmonic mean equations, respectively.

$$Q_{eff} = \sum_m C_m Q_{Ni-m} \tag{10}$$

$$D_{0,eff} = \frac{1}{\sum_m \frac{C_m}{D_{0,Ni-m}}} \tag{11}$$

Q_{Ni-m} and $D_{0,Ni-m}$ are the activation energy and pre-exponential factor of element *m* and Ni interdiffusion coefficient (chemical diffusivity). Through these equations, composition sensitivity is captured and contribution of each element to the effective values is balanced by their atomic concentration, C_m.

In this study, estimation of the interdiffusion coefficient of the Ni-m binary systems is carried out using DICTRA interfaced with Thermo-Calc. The details of the computation procedure are discussed in the next section.

4. COMPUTATIONAL VERIFICATION OF EXPERIMENTS USING DICTRA

DICTRA is a software package for simulation of diffusion-controlled processes such as homogenization of alloys, micro-segregation during solidification and coarsening of precipitates in multicomponent alloys through the numerical application of Fick-Onsager law [34, 35].

$$\tilde{J}_i = -\sum_{j=1}^{n-1} \tilde{D}_{ij} \frac{\partial c_j}{\partial z} \quad (12)$$

where $\tilde{J}_i$ is the atomic flux and $\tilde{D}_{ij}$ is (n-1)^2 temperature and composition dependent diffusivity matrix.

The simulations retrieve data from thermodynamic and mobility databases that have been developed based on CALPHAD method [36]. This method models the Gibbs energy of phases as a function of composition, temperature and pressure and uses the available experimental and theoretical data to assess the parameters of the models [34, 37]. The accuracy of the simulations strongly depends on the quality of these data. Many researchers have developed the databases for various elements including Ni [38-42]. In the present work, TCNi5 [43] thermodynamic and MOBNi2 [44] mobility databases have been used to determine the composition-sensitive effective diffusivity.

4.1 Volume fraction and composition segregation study

, Since diffusion in the γ' ordered phase is much slower than in the disordered γ channels [26], during diffusion-controlled processes such as coarsening, effective diffusion takes place in the γ channels. In order to define the binary systems with compositions corresponding to the channels, the concentration profile of the elements in the γ/γ' phases needs to be determined. There are a number of assumptions associated with the simulations performed in DICTRA to estimate the segregation of the elements: (i) only substitutional atoms contribute to the total volume of the element and (ii) all the atoms in the systems are substitutional. Results of compositional segregation are shown in Figure 12 at 1000 °C. It is evident that elements such as Cr, Co and Re tend to partition in γ channels while Al, Ti and Ta are segregated in γ' phase to form the ordered phase. Therefore, a compositional gradient is expected to exist at the interface, which is the subject of the research on the interfacial diffusion as a dominant mechanism controlling coarsening [29].

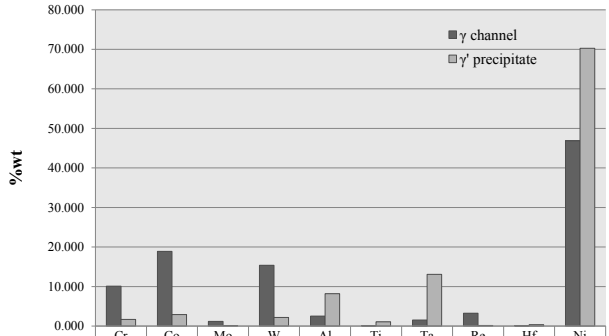

	Cr	Co	Mo	W	Al	Ti	Ta	Re	Hf	Ni
γ channel	10.110	18.900	1.170	15.380	2.540	0.024	1.510	3.250	0.016	46.870
γ' precipitate	1.690	2.890	0.130	2.180	8.180	1.060	13.090	0.140	0.340	70.270

Figure 12 Elemental segregation in γ channel and γ' precipitates.

According to the listed assumptions, the volume fraction of the γ' phase is defined by,

$$V_f = \frac{\sum_i n_i(\gamma')}{\sum_i n_i} \quad (13)$$

where $n_i(\gamma')$ is the number of moles of element *i* in the γ' phase and n_i is the total number of moles defined in the system.The results are in good agreement with observations in the literature which show that the volume fraction remains constant within aging conditions [29]. Moreover, this was also observed from SEM micrographs through the 1-point correlation function which showed no variation in volume fraction of precipitates after stress-assisted and stress-free aging. However, it is known that the equilibrium γ' volume fraction is lower at elevated temperatures. Computations performed in DICTRA showed a drop in volume fraction at temperatures above 1000 °C. Note that the results are based on pure thermodynamic equilibrium conditions and do not include the kinetics by which the equilibrium state is reached.

4.2 Effective diffusivity

Ni-m binary systems were defined based on the study conducted in the previous section. Interdiffusion coefficients of the binary systems were obtained from the MOBNi2 mobility database in the temperature range of 700°C to 1100°C after computing the equilibrium states. By fitting the chemical diffusivity values to an Arrhenius type relation as a function of temperature, the desired diffusion parameters including Q_{Ni-m} and $D_{0,Ni-m}$ were acquired for all binary systems which are summarized in Table 4. The values of the effective diffusivity parameters of equation (9) were estimated using equations (10) and (11). The values of the effective activation energy and effective pre-exponential factor for CMSX-8 were calculated to be 274.7 *kJ/mol* and 1.09×10^{-7} m^2/s, respectively. The value of the effective activation energy is in the order of reported experimental coarsening activation energy. A recent study was conducted on CMSX-4 using the experimental diffusivity

of binary systems. Based on the corresponding composition of CMSX-4, Q_{eff} was calculated to be 271.73 *kJ/mol* and according to literature it is close to the Q_{exp} of 272.40 *kJ/mol* [33].

Table 4 Calculated $\boldsymbol{Q_{Ni-m}}$ and $\boldsymbol{D_{0,Ni-m}}$ for the interdiffusion of element *m* in Ni.

	$Q_{Ni,m}$(*kJ/mol*)	$D_{0\ Ni,m}$(m^2/s)
Ni-Cr	280	2.42×10^{-4}
Ni-Co	294	3.30×10^{-4}
Ni-Mo	282	2.01×10^{-4}
Ni-W	288	6.77×10^{-5}
Ni-Al	257	1.69×10^{-4}
Ni-Ti	259	1.10×10^{-4}
Ni-Ta	267	7.05×10^{-5}
Ni-Re	285	8.67×10^{-6}
Ni-Hf	252	1.91×10^{-4}
Ni-Ni	265	5.64×10^{-8}

Evaluation of the effective activation energy as a composition dependent parameter enables us to predict the coarsening behavior of the material with respect to compositional variation. The study on the influence of reduction in Re content on second generation single-crystal Ni-base superalloys is an ongoing research effort and the detailed approach proposed in this work provides the capability to predict the microstructure degradation response at elevated temperatures.

5. CONCLUSIONS AND CONTRIBUTIONS

1. The state of the aged microstructure was shown to be rapidly characterized using high resolution digital images and analyzed by 2-point correlation method which is a rigorous method to quantitatively describe the state of the aged microstructure. This method was used to measure γ' precipitate size and γ channel width of aged microstructures in a statistical manner and provided higher reliability than traditional quantification methods such as line intercept.

2. Rafting and coarsening of the microstructure occurs simultaneously during aging conditions. Therefore, stress-assisted and stress-free aging experiments were designed to distinguish these two processes and characterize the response under the influence of each. Tapered specimens provided the capability to study isothermal stress-assisted aging behavior in a continuous range of stress levels and to characterize the kinetics of raft formation as a function of temperature and stress. A phenomenological relation that had been derived for CMSX-4 was employed to describe the kinetics of rafting using the rate of γ channel widening as the representative microstructure feature to capture the degree of rafting. The relation was capable of predicting the behavior of CMSX-8 below the saturation level where a fully rafted state was reached. Comparing to CMSX-4, as one would expect, reduced Re content in CMSX-8 resulted in accelerated rafting kinetics and lower activation energy.

3. Short-term stress-free experiments were conducted on CMSX-8 at different temperatures to evaluate the coarsening process occurring during rafting independently. The coarsening of γ' precipitates was found to follow the LSW model. No coalescence and morphology evolution to irregular shapes were observed under the test conditions and precipitates were partially coherent. As long as the LSW model is obeyed, the mechanism of coarsening is volume diffusion and coherency of precipitates is retained. The coarsening activation energy for CMSX-8 was calculated to be in the vicinity of CMSX-4 and other Ni-base alloys.

4. DICTRA, interfaced with Thermo-Calc, was used as a computational tool to calculate the effective diffusivity and activation energy of CMSX-8. The value of 274.7 *kJ/mol* for effective activation energy, verifies the coarsening activation energy of 269.4 *kJ/mol* obtained experimentally. This computational methodology enables the prediction of the compositional sensitivity of the aging kinetics. Therefore, it can be potentially utilized for other alloying systems to predict the diffusion-controlled processes.

ACKNOWLEDGEMENTS

This work is supported by U.S. Department of Energy, National Energy Technology Laboratory, University Turbine Systems Research (UTSR) Program, Grant DE-FE0011722, and Siemens Energy Inc., Orlando, FL.

REFERENCES

1. Wahl, J.B. and K. Harris, *New single crystal superalloys, CMSX-7 and CMSX-8.* Superalloys 2012, 2012: p. 179-188.
2. Nabarro, F.R.N., *Rafting in superalloys.* Metallurgical and Materials Transactions a-Physical Metallurgy and Materials Science, 1996. 27(3): p. 513-530.
3. Reed, R.C., *The superalloys fundamentals and applications*. 1st ed. 2006: Cambridge University press.
4. Matan, N., D.C. Cox, C.M.F. Rae, and R.C. Reed, *On the kinetics of rafting in CMSX-4 superalloy single crystals.* Acta Materialia, 1999. 47(7): p. 2031-2045.
5. Lifshitz, I.M. and V.V. Slyozov, *The kinetics of precipitation from supersaturated solid solutions.* Journal of Physics and Chemistry of Solids, 1961. 19(1-2): p. 35-50.
6. Wagner, C., Z Elektrochem, 1961. 65(581).
7. Baldan, A., *Review Progress in Ostwald ripening theories and their applications to nickel-base superalloys - Part I: Ostwald ripening theories.* Journal of Materials Science, 2002. 37(11): p. 2171-2202.
8. Andersson, J.O., T. Helander, L.H. Hoglund, P.F. Shi, and B. Sundman, *THERMO-CALC & DICTRA, computational tools for materials science.* Calphad-Computer Coupling of Phase Diagrams and Thermochemistry, 2002. 26(2): p. 273-312.
9. Fullwood, D.T., S.R. Niezgoda, B.L. Adams, and S.R. Kalidindi, *Microstructure sensitive design for performance optimization.* Progress in Materials Science, 2010. 55(6): p. 477-562.
10. Niezgoda, S.R., D.T. Fullwood, and S.R. Kalidindi, *Delineation of the space of 2-point correlations in a composite material system.* Acta Materialia, 2008. 56(18): p. 5285-5292.
11. Fullwood, D.T., S.R. Kalidindi, S.R. Niezgoda, A. Fast, and N. Hampson, *Gradient-based microstructure reconstructions from distributions using fast Fourier transforms.* Materials Science and Engineering: A, 2008. 494(1–2): p. 68-72.
12. Fullwood, D.T., S.R. Kalidindi, S.R. Niezgoda, A. Fast, and N. Hampson, *Gradient-based microstructure reconstructions from distributions using fast Fourier transforms.* Materials Science and Engineering a-Structural Materials Properties Microstructure and Processing, 2008. 494(1-2): p. 68-72.
13. Adams, B.L., S.R. Kalidindi, and D.T. Fullwood, *Chapter 12 - Higher-Order Microstructure Representation*, in *Microstructure Sensitive Design for Performance Optimization*, B.L.A.R.K.T. Fullwood, Editor. 2013, Butterworth-Heinemann: Boston. p. 249-268.
14. Kirka, M.M., *Thermomechanical behavior of a directionally solidified nickel-base superalloy in the aged state*, in *Woodruff school of mechanical engineering*. 2014, Georgia Institute of Technology.
15. Ignat, M., J.Y. Buffiere, and J.M. Chaix, *Microstructures induced by a stress gradient in a Nickel-based superalloy*. Acta Metallurgica Et Materialia, 1993. 41(3): p. 855-862.
16. Tinga, T., W.A.M. Brekelmans, and M.G.D. Geers, *Directional coarsening in nickel-base superalloys and its effect on the mechanical properties.* Computational Materials Science, 2009. 47(2): p. 471-481.
17. Epishin, A., T. Link, M. Nazmy, M. Staubli, H. Klingelhoffer, and G. Nolze, *Microstructural degradation of CMSX-4: Kinetics and effect on mechanical properties.* Superalloys 2008, 2008: p. 725-731.
18. Serin, K., G. Gobenli, and G. Eggeler, *On the influence of stress state, stress level and temperature on gamma-channel widening in the single crystal superalloy CMSX-4.* Materials Science and Engineering a-Structural Materials Properties Microstructure and Processing, 2004. 387: p. 133-137.
19. Giamei, A.F. and D.L. Anton, *Rhenium additions to a Ni-base superalloy: Effects on microstructure.* Metallurgical Transactions A, 1985. 16(11): p. 1997-2005.
20. Blavette, D., P. Caron, and T. Khan, *An atom-probe study of some fine-scale microstructural features in Ni-based single crystal superalloys*, in *Superalloys 1988* D.N.D. S. Reichman, G. Maurer, S. Antolovich, C. Lund, Editor., The Metallurgical Society of AIME. p. 305-314.
21. Mushongera, L.T., M. Fleck, J. Kundin, Y. Wang, and H. Emmerich, *Effect of Re on directional gamma '-coarsening in commercial single crystal Ni-base superalloys: A phase field study.* Acta Materialia, 2015. 93: p. 60-72.
22. Li, H.Y., L.L. Zuo, X.P. Song, Y.L. Wang, and G.L. Chen, *Coarsening behavior of gamma ' particles in a nickel-base superalloy.* Rare Metals, 2009. 28(2): p. 197-201.
23. Hadjiapostolidou, D. and B.A. Shollock, *Long term coarsening in Rene 80 Ni-base superalloy*. Superalloys 2008, ed. R.C. Reed, K.A. Green, P. Caron, T.P. Gabb, M.G. Fahrmann, and E.S. Huron. 2008, Warrendale: Minerals, Metals & Materials Soc. 733-739.
24. Lapin, J., M. Gebura, T. Pelachova, and M. Nazmy, *Coarsening kinetics of cuboidal gamma ' precipitates in single crystal nickel base superalloy CMSX-4.* Kovove Materialy-Metallic Materials, 2008. 46(6): p. 313-322.
25. Mackay, R.A. and M.V. Nathal, *Gamma-' coarsening in high-volume fraction Nickel-base alloys* Acta Metallurgica Et Materialia, 1990. 38(6): p. 993-1005.
26. Ardell, A.J. and V. Ozolins, *Trans-interface diffusion-controlled coarsening.* Nature Materials, 2005. 4(4): p. 309-316.
27. Epishin, A., T. Link, U. Bruckner, B. Fedelich, and P. Portella, *Effects of segregation in nickel-base superalloys: Dendritic stresses*. Superalloys 2004, ed. K.A. Green, T.M. Pollock, H. Harada, T.E. Howson, R.C. Reed, J.J. Schirra, and S. Walston. 2004, Warrendale: Minerals, Metals & Materials Soc. 537-543.
28. Tang, S., Z. Zheng, and L.K. Ning, *Gamma prime coarsening in a nickel base single crystal superalloy.* Materials Letters, 2014. 128: p. 388-391.
29. Tiley, J., G.B. Viswanathan, R. Srinivasan, R. Banerjee, D.M. Dimiduk, and H.L. Fraser, *Coarsening kinetics of gamma ' precipitates in the commercial nickel base Superalloy Rene 88 DT.* Acta Materialia, 2009. 57(8): p. 2538-2549.
30. Paul, A., T. Laurila, V. Vuorinen, and S.V. Divinski, *Thermodynamics, Diffusion and the Kirkendall Effect in Solids*. 2014: Springer.
31. Ges, A.M., O. Fornaro, and H.A. Palacio, *Coarsening behaviour of a Ni-base superalloy under different heat treatment conditions.* Materials Science and Engineering a-Structural Materials Properties Microstructure and Processing, 2007. 458(1-2): p. 96-100.
32. Zhao, S.Q., X.S. Xie, G.D. Smith, and S.J. Patel, *Gamma prime coarsening and age-hardening behaviors in a new nickel base superalloy.* Materials Letters, 2004. 58(11): p. 1784-1787.
33. Ai, C., X.B. Zhao, J. Zhou, H. Zhang, L. Liu, Y.L. Pei, S.S. Li, and S.K. Gong, *Application of a modified Ostwald ripening theory in coarsening of gamma ' phases in Ni based single crystal superalloys.* Journal of Alloys and Compounds, 2015. 632: p. 558-562.
34. Borgenstam, A., A. Engstrom, L. Hoglund, and J. Agren, *DICTRA, a tool for simulation of diffusional transformations in alloys.* Journal of Phase Equilibria, 2000. 21(3): p. 269-280.

35. Wang, C.P., L.N. Yan, J.J. Han, and X.J. Liu, *Diffusion mobilities in the fcc Ag-Cu and Ag-Pd alloys.* Calphad-Computer Coupling of Phase Diagrams and Thermochemistry, 2012. 37: p. 57-64.
36. Agren, J., *Calculation of phase diagrams: Calphad.* Current Opinion in Solid State & Materials Science, 1996. 1(3): p. 355-360.
37. Lukas, H., S.G. Fries, and B. Sundman, *Computational thermodynamics - The Calphad method*. 2007: Cambridge university press.
38. Campbell, C.E., W.J. Boettinger, and U.R. Kattner, *Development of a diffusion mobility database for Ni-base superalloys.* Acta Materialia, 2002. **50**(4): p. 775-792.
39. Kroupa, A., *Modelling of phase diagrams and thermodynamic properties using Calphad method - Development of thermodynamic databases.* Computational Materials Science, 2013. 66: p. 3-13.
40. Cao, Z.M., X. Shi, W. Xie, I. Ohnuma, K. Ishida, and Z.Y. Qiao, *Thermodynamic reassessment of Ni-Ga binary system.* Rare Metals, 2015. 34(12): p. 864-872.
41. Zhou, Z., Y.J. Liu, G. Sheng, F.Y. Lei, and Z.T. Kang, *A contribution to the Ni-based mobility database: Fcc Ni-Fe-Ti ternary alloy.* Calphad-Computer Coupling of Phase Diagrams and Thermochemistry, 2015. 48: p. 151-156.
42. Liu, X.J., H.H. Hu, J.J. Han, Y. Lu, and C.P. Wang, *Assessment of the diffusional mobilities in fcc Ni-Nb and fcc Ni-Mo alloys.* Calphad-Computer Coupling of Phase Diagrams and Thermochemistry, 2012. 38: p. 140-145.
43. Thermo-Calc, Stockholm, Sweden, TCNi5, thermodynamic database fo Ni, version 5.0.
44. Thermo-Calc, Stockholm, Sweden, MOBNi2, mobility database fo Ni, version 2.0.

APPENDIX 2

ON THE DEVELOPMENT OF ICME TOOLS FOR CREEP AND AGING OF CMSX®-8

E.A. Estrada Rodas[1], S. Gorgannejad[1], R.W. Neu[1,2], Z. Dyer[3], P.M. Draa[4], and S.R. Shinde[3]
[1]The George W. Woodruff School of Mechanical Engineering, Georgia Institute of Technology, Atlanta GA
[2]School of Materials Science and Engineering, Georgia Institute of Technology, Atlanta, GA
[3]Siemens Energy Inc., Orlando FL
[4]Siemens Energy Inc., Charlotte, NC

Keywords: aging, creep, crystal viscoplasticity, diffusivity, Ni-base superalloy, rafting

Abstract

In this paper three different tools are developed to aid Integrated Computational Materials Engineering (ICME) of Ni-base superalloys for next generation industrial gas turbines: (i) models to predict the state of the γ/γ' structure through modeling of the kinetics of aging, including both rafting and coarsening, (ii) a crystal viscoplasticity (CVP) model for determining the creep and cyclic deformation response that uses the current state of the γ/γ' structure as is an input, and (iii) the use of computational thermodynamics and kinetics software for multi-component systems to determine how diffusivity, which is a key parameter in the aging and in viscoplasticity models, is altered with variations in composition of the γ and γ' phases. Experiments are conducted on a reduced Re content superalloy, CMSX®-8, to determine the parameters of the aging and crystal viscoplasticity models.

Introduction

During this past decade, next generation industrial gas turbines (IGT) have been moving toward the employment of single crystal blades, which are now ubiquitous in aerospace gas turbine propulsion systems. Second generation single crystal (SX) superalloys commonly used in current generation aerospace propulsion systems (CMSX-4®, PWA1484, René N5) contain 3 wt% Re, which reduces creep deformation in the γ channels and maintains the stability of the microstructure. Consequently, these second generation superalloys have become the benchmark in the development of superalloys more suitable for IGT applications that are characterized by considerably larger blade sizes and cross sections and longer operational times. The cost of the rare elements, specifically Re, is one of the limiting constraints in selecting these superalloys for IGT applications. In addition, there are challenges in developing casting protocols for these larger sectioned components that have propensity for developing casting anomalies and microstructure variations through the blade and its platform. Consequently, there is a large push to develop SX superalloys with no or reduced Re content that have properties suitable for IGT applications.

Recently Cannon-Muskegon introduced a SX superalloy, denoted CMSX®-8, with Re reduced to 1.5 wt.%, but otherwise similar in composition to the benchmark superalloy CMSX-4® [1]. Initial mechanical property studies conducted on this new superalloy show minimal reduction in creep and fatigue properties compared to the benchmark [1]. Since IGT must operate at sustained loads and temperatures for extremely long times, the aging of the alloy and its impact on mechanical behavior including long-term creep-fatigue interactions and thermomechanical fatigue needs to be well understood and predicted when designing components. It is thought that the Re plays a role in this long-term behavior and initial studies to date cannot readily capture these effects.

This paper explores the development of integrated computational materials engineering (ICME) tools for predicting the impact of reducing Re on the degradation and mechanical behavior of these superalloys under service conditions. In particular, this study is aimed at expanding knowledge of longer-term degradation of CMSX®-8 through aging and characterization studies. The end goal is to develop a microstructure-sensitive constitutive model that can be used to predict the response of components under realistic IGT conditions. This project is split into several facets. The first one involves establishing the kinetics of aging of the microstructure with the objective of determining how rapidly the microstructure evolves under service conditions and developing models that can predict the state of the γ/γ' structure. The second facet consists of developing a physics-based constitutive model that captures relevant microstructure attributes to enable thermomechanical analysis of realistic geometries. The third facet consists of exploring the use of thermodynamics and kinetics software such as Thermo-Calc and DICTRA (DIffusion Controlled TRAnsforamtions), to model diffusion-controlled microstructure evolution and to determine how variations in the elemental composition, both in γ channels and γ' particles, affect the diffusivity that is implicitly embedded in the coefficients of the rate equation in the crystal viscoplasticity model. The aim is to explore whether the variances in the long-term creep and aging behavior due to reducing the Re content can be captured in constitutive models by accounting for differences in diffusivity in the aging kinetics and flow rule.

Material description

The material investigated is CMSX-8[B/C] which contains intentional additions of boron and carbon to improve castability and machinability [2]. The nominal composition of this alloy can be found in reference [3]. The CMSX-8 rods used in this research were cast by PCC Airfoils and then solution and double age treated using proprietary conditions typical for blade components. The initial γ/γ' microstructure of this alloy is shown in Figure 1.

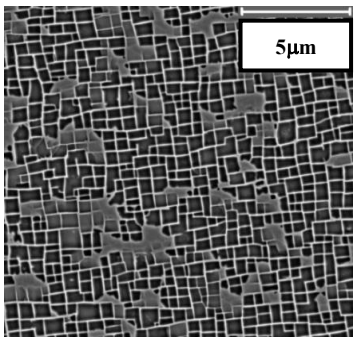

Figure 1. SEM image of as-received microstructure of CMSX-8.

In this work, for simplicity we will refer to CMSX-8[B/C] as CMSX-8. The volume fractions of the γ and γ' phases were estimated to be 0.27 and 0.73, moreover the average γ channel width and γ' size, were estimated to 0.14 μm and 0.74 μm, respectively, these values were obtained using techniques derived from two-point statistics [4, 5]. The dendritic arm spacing and the secondary dendritic arm spacing were measured using SEM images, and were estimated to 436 ± 150 μm and 112 ± 37 μm, respectively which are comparable to the measured dendritic arm spacing of other Ni-based superalloys [6, 7].

Aging studies on the <001> oriented single crystal CMSX-8

During high temperature service conditions (the temperature of the gas stream is about 1477 °C [8]), single crystal gas turbine blade materials, subjected largely to centrifugal forces resulting from significant rotational speeds, are prone to severe microstructural degradation. The combined influence of stress and temperature, results in an evolution of the γ/γ′ microstructure to a rafted microstructure marked by horizontal or vertical γ channels widening and γ′ precipitates elongation and coalescence which ultimately leads to topological inversion of the microstructure. The mechanisms of failure under creep in an evolved microstructure will differ from the initial microstructure and therefore understanding the kinetics of this process is important. In this work, the kinetics of microstructural evolution of CMSX-8 under high temperature and low stress levels that result in a rafted microstructure is characterized by an empirical model adopted from Epishin et al. for CMSX-4® [9].

The thermodynamic driving force for rafting is impacted by the applied stress (σ) and by the misfit stresses as well as the anisotropy of the resulting dislocation debris fields. The misfit stresses are induced by the γ and γ′ lattice parameter difference, denoted as lattice misfit, and is defined by [10],

$$\delta = \frac{2\left(a_{\gamma'} - a_{\gamma}\right)}{a_{\gamma'} + a_{\gamma}} \qquad (1)$$

where $a_{\gamma'}$ and a_{γ} are γ′ precipitate and γ channel lattice parameters, respectively. Cubic precipitates in alloys with negative lattice misfit elongate perpendicular to the loading direction under tensile stress (N-type rafts) while they coalesce in loading direction under compressive stresses (P-type rafts). Most modern Ni-base superalloys, including CMSX-8, used in hot gas path sections are negative misfit alloys [10].

Experimental procedure and microstructure characterization

To investigate the kinetics of microstructure degradation as a function of applied stress and temperature, specimens with a tapered geometry and circular cross section were used to create a linear stress gradient along the sample. The cross section diameter varies from 12.7 mm to 6.35 mm within a 50.8 mm length. Hence the applied stress level changes by a factor of four at the two ends of the specimen. This method provides the means to rapidly characterize the stress dependence of microstructure evolution in a single specimen. To examine the γ/γ′ microstructure within the core dendritic region, microscopy was performed using a TESCAN MIRA3 XM SEM at 10kV. For image quantification purposes, the two-point correlation technique was used. The two-point correlation functions are statistical microstructure descriptors that provide the tools to characterize spatial arrangement and anisotropy of microstructural attributes. The two-point correlation function captures the probability density that a randomly located vector of length ***r*** has its head and tail in a specific local sate and is mathematically represented by [11],

$$f\left(h, h' \mid \mathbf{r}\right) = \frac{\iiint_{x \in \Omega \mid \mathbf{r}} m(\mathbf{x}, h)\, m(\mathbf{x}+\mathbf{r}, h')\, d\mathbf{x}}{vol\left(\Omega \mid \mathbf{r}\right)} \qquad (2)$$

where Ω is the spatial domain, h is the local state of interest and m is the microstructure function representing the volume density of local state that is normalized by the volume of the region. The microstructural features of interest in this study are size and morphology of γ channels and γ′ precipitates. A MATLAB® routine was developed that uses digital binary images and processes them by two-point correlation method. Quantification of microstructures was performed on specimens subjected to isothermal aging under different stress levels and dwell times. Epishin et al. [9] proposed that γ channel widening during rafting represents the degree of microstructure degradation under stress-assisted aging condition. Therefore, measurement of kinetics of channel widening provides the means to characterize the extent microstructure evolution by rafting.

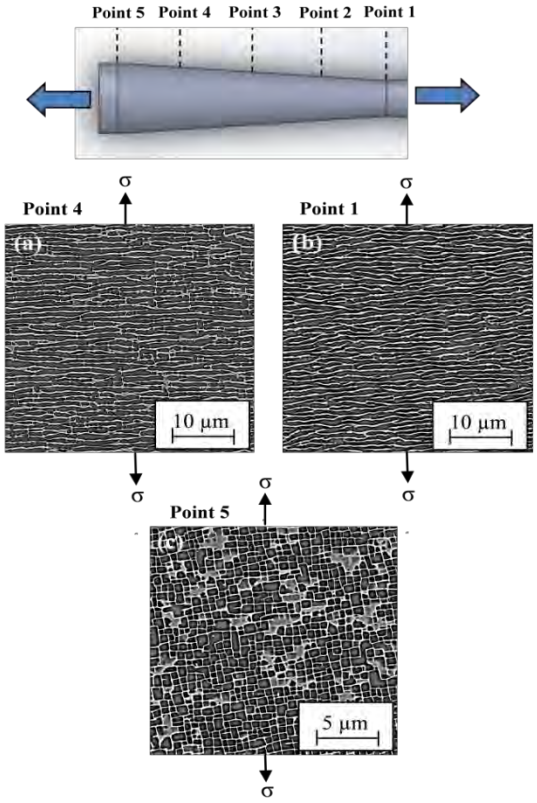

Figure 2. SEM images showing different stages of rafting:
(a) 34 MPa, 1120 °C, 50 hours, (b) 100 MPa, 1120 °C, 50 hours, (c) 38 MPa, 950°C, 445 hours.

Mechanism of rafting

By application of an external tensile stress along the γ′ cube axis, the primary slip systems in the γ channels are activated and *a/2*<110>{111}creep dislocations begin to glide in the channels. The movement of the dislocations is under the influence of the applied stress and the misfit stresses simultaneously. In absence of external stress, misfit stresses at the γ/γ′ horizontal and vertical

interfaces are equally distributed. However, the application of external stress will induce a gradient of misfit stresses between the faces of the same precipitate in the vertical and in the highly stressed horizontal channels. The influence of mobile dislocations in the γ channels generally relieves these misfit stresses. Dislocations glide from locations with low misfit stress to locations with high misfit stress and are then absorbed by the horizontal γ/γ′ interfaces. The formation of dislocation networks at the interface results in loss of coherency which causes relaxation of the misfit stresses in the horizontal channels while the vertical channels remain coherent [12, 13]. Rafting is a sequential process and requires a certain amount of plastic deformation (0.1% for CMSX-4® at 950 ºC [14]) in the γ channel, glide of creep dislocations and subsequent loss of coherency. Dislocation networks provide the diffusional path for atoms to travel. The driving force for mass transport is driven by the chemical potential gradient causing the interchange of the neighboring atoms. Therefore, γ partitioning alloying elements such as Cr, Co, and Re diffuse to the horizontal channels and on the other hand γ′ partitioning elements such as Al and Ti travel to vertical channels [15].

Isothermally aged microstructures are shown in Figure 2. Because of the negative lattice misfit under tensile stress, elongation of the precipitates has occurred normal to the loading direction and the rafted microstructure is clearly observed, particularly when the temperature is sufficiently high as in Figure 2(a) and 2 (b). At the lower temperature of 950 °C with dwell time of 445 hours and similar stress level as in Figure 2(a), there is no apparent morphology change (Figure 2(c)). Rafting is a diffusion-controlled process which is thermally activated. Consequently, the impact of temperature on the state of microstructure is more pronounced.

The volume fraction of the γ′ precipitates remains constant as the morphology changes. This has been addressed by a number of authors experimentally and computationally [9, 12, 13]. The elongation of the precipitates in the horizontal direction is associated with its shrinkage in the vertical direction and therefore widening of the γ channels is imposed geometrically. The shrinkage of the vertical channels, which is compensated by the horizontal channel widening, proceeds until the vertical channels disappear completely and the microstructure reaches the fully rafted state (Figure 2 (b)). Extensive rafting and formation of links between precipitates will eventually lead to the inversion of the γ/γ′ microstructure such that the discontinued disordered γ phase is distributed in the ordered γ′ matrix phase which substantially affects the activity of the dislocations [10].

Kinetics of rafting

The experimental results from rafting tests have been shown to follow a phenomenological Arrhenius type relation [9],

$$\dot{w}_{raft}(T,\sigma) = A\exp\left(-\frac{Q-U(T)\sigma}{kT}\right) \quad (3)$$

where A is a pre-exponential factor, Q is the rafting activation energy, σ is applied stress, k is universal gas constant, T is the absolute temperature and U(T) is temperature dependent function defined as,

$$U(T) = U_T\left\langle T - T_o\right\rangle^n \quad (4)$$

The exponent n and the coefficient U_T are fit to experiments. The reference temperature T_o is the temperature below which no rafting occurs. For a best fit, this value for CMSX-8 was found to be 850 °C which is close to the CMSX-4® reference temperature of 828 °C [9].

Figure 3 shows the increase in channel widening rate versus stress at temperatures of 900°C, 950°C, and 1120°C. The model parameters are given in Table I. A rafting activation energy of 206 *kJ/mol* is calculated for CMSX-8. This value is lower than the rafting activation energy for CMSX-4® (222 *kJ/mol*) [9] and is consistent with the greater Re content of CMSX-4®.

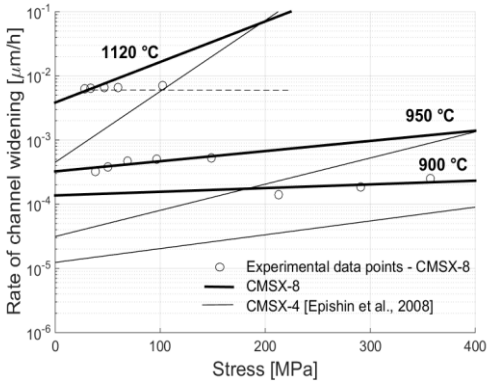

Figure 3. The kinetics of γ channel widening in [001] oriented single crystal, CMSX-8.

Table I. Rafting kinetics model parameters, CMSX-8

A (μm/h)	Q (kJ/mol)	U_T(J/mol.MPa.K^n)	n
2.0×10^5	206	0.033	1.525

The model is in good agreement with the experimental data except at the highest temperature of 1120 °C. At this temperature, the experimental data points follow the horizontal dashed line which represents a saturation level of the microstructure evolution as the fully rafted microstructure is reached at all stress levels. Beyond saturation level, rafting is decelerated and isotropic coarsening becomes the dominant process. It is suggested that the approximate value of $3w_0$ for channel width size is the criterion which defines the completion of rafting [9]. This gives the final channel width equal to 0.42 μm for CMSX-8.

Crystal viscoplasticity model for creep

In this section a physics-based crystal viscoplasticity (CVP) model is described that is capable of predicting the creep deformation response of CMSX-8. To capture the highly anisotropic inelastic behavior of single crystal alloys, at each material point, the orientation of the crystal lattice is prescribed to track the collective dislocation motion on each slip system, explicitly defined by a slip plane and a slip direction [16]. In general for Ni-base superalloys, three families of slip systems may be activated in the γ and γ' phases in face-centered cubic lattices, these include the 12 primary octahedral slip systems <110>{111}, the 12 secondary octahedral slip systems <112>{111} (shear acting on partial dislocations in γ' precipitates), and 6 cube slip systems <110>{001}. The primary octahedral slip occurs on the close-packed planes and is active over the entire temperature range. The secondary octahedral slip systems are important to consider when conditions are ripe for dislocations to cut through the γ' precipitates since dislocations split into Shockley partial dislocations and the resolved shear stress on the partials becomes an important driver. Macroscopic cube slip may only be active at

higher temperatures. Microscopic cube slip has been observed only occasionally while zig-zag octahedral slip in the γ channels is a major source of macroscopic cube slip [17]. Since only the <001> crystallographic orientation is examined in the current investigation, only dislocation motion to the primary and secondary slip systems will be addressed.

Constitutive relations and flow rules

In continuum crystal plasticity formulations –where symbols in bold represent tensors- the inelastic part of the deformation gradient $\boldsymbol{F}^{in}$ is determined from the macroscopic inelastic velocity gradient which is the aggregate sum of the inelastic shear strain rate $\dot{\gamma}^{in(\alpha)}$ on all possible slip systems α,

$$\mathbf{L}^{in} = \dot{\mathbf{F}}^{in}\,\mathbf{F}^{in^{-1}} = \sum_{\alpha=1}^{N_{slip}} \dot{\gamma}^{in(\alpha)} \left(\hat{\mathbf{d}}_o^{(\alpha)} \otimes \hat{\mathbf{n}}_o^{(\alpha)} \right) \qquad (5)$$

where $\hat{\mathbf{d}}_o^{(\alpha)}$ and $\hat{\mathbf{n}}_o^{(\alpha)}$ are the slip direction and slip plane normal unit vectors, respectively, defined in the reference configuration for each slip system, and N_{slip} is the number of possible active slip systems. In Ni-base superalloys single crystals, dislocation slip is either limited to the γ channels or cutting through the γ' particles. Consequently, the driver for inelastic shear strain rate is different whether the γ' precipitate can be cut or not. Therefore the inelastic velocity gradient is additively decomposed into two terms corresponding to the relevant deformation mechanisms that are active at each phase:

$$\mathbf{L}^{in} = f_{\gamma} \left(\sum_{\alpha=1}^{12} \dot{\gamma}_{\gamma}^{in(\alpha)} \left(\hat{\mathbf{d}}^{(\alpha)} \otimes \hat{\mathbf{n}}^{(\alpha)} \right) \right) + f_{\gamma'} \left(\sum_{\alpha=13}^{24} \dot{\gamma}_{L1_2}^{in(\alpha)} \left(\hat{\mathbf{d}}^{(\alpha)} \otimes \hat{\mathbf{n}}^{(\alpha)} \right) \right) \qquad (6)$$

where f_{γ} and $f_{\gamma'}$ are the volume fractions of the γ and γ' phases, respectively. Here, the slip plane is assumed to be octahedral for all slip systems; i.e., $\hat{\mathbf{n}}^{(\alpha)} \parallel \{111\}$. Therefore in γ, the primary octahedral slip systems operate, $\hat{\mathbf{d}}^{(\alpha)} \parallel <110>$, while dislocations cutting through γ' depend on shear stress acting on partial dislocations necessary to cut through the ordered structure that manifests as ribbon shearing; hence, $\hat{\mathbf{d}}^{(\alpha)} \parallel <112>$ for $13 \le \alpha \le 24$. Splitting the dislocation mechanisms in $\boldsymbol{L}^{in}$ enables the model to be sensitive to volume fraction size and morphology of the γ/γ' microstructure. This is critical for the prediction of the different aspects of the creep response that vary depending on temperature and stress [8, 17-19]. In particular, features of incubation, primary creep, tertiary creep, and rafting can be addressed. Secondary creep appears at the saturation point when the γ channels have been completely filled with dislocations [20]. We compared CMSX-8 creep responses to CMSX-4® [8], Figure 4, and found that dominant mechanisms in CMSX-8 also appear to partition into the same temperature and stress regimes as CMSX-4®.

Inelastic shear strain rate relations

The physics-based constitutive model is founded on a crystal viscoplasticity and damage formulation originally developed by Ma, Dye, and Reed [19]. In this work, the model is extended to CMSX-8, the backstress is reformulated, and a diffusivity parameter is added to study the effect of composition on creep behavior. Specifically, the effect Re content of the alloy by using an Arrhenius type diffusivity parameter is studied.

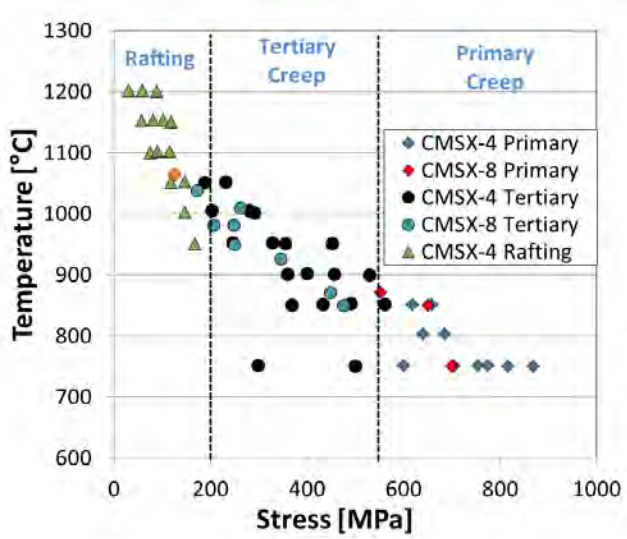

Figure 4. Temperature and stress dependence on the characteristic deformation mechanism.

The relationship between the inelastic strain rates and the density of mobile dislocation is assumed to follow the Orowan equation. In the γ channels the flow rule for each primary slip system is described by:

$$\dot{\gamma}_{\gamma}^{in(\alpha)} = \rho_{\gamma}^{(\alpha)} b \lambda_{\gamma}^{(\alpha)} F_{attack} \Theta(T,\xi) \exp\left\{ \frac{-Q_{slip}^{110} + \left(\left| \tau_{eff_{\gamma}}^{(\alpha)} \right| - \kappa_{\gamma}^{(\alpha)} \right) V_{c1}^{(\alpha)}}{kT} \right\} sign\left(\tau_{eff_{\gamma}}^{(\alpha)} \right) \qquad (7)$$

The activation energy Q_{slip}^{110} represents the thermal component for overcoming the obstacles in absence of stress which is similar to activation energy for self-diffusion. The coefficients before the exponential represents the mobile dislocation density on that slip system, the Burger's vector, and the dislocation vibration frequency, which is less than the Debye frequency, and

$$\lambda_{\gamma}^{(\alpha)} = c_{jump1} \left(\frac{1}{L_{\gamma}} + \frac{1}{L_{\rho}^{(\alpha)}} \right)^{-1} \qquad (8)$$

defines the dislocation mean free path (jump distance) which is inversely proportional to the dislocation pinning spacing in the γ phase, here with components due to pinning at the γ/γ' interfaces (hence, associated to width of γ channel) and average spacing of forest dislocations,

$$L_{\rho}^{(\alpha)} = \frac{c_{Fdisl}}{\sqrt{\rho_F^{(\alpha)}}} \qquad (9)$$

The dislocation mean free path is an average measure of the distance travelled by a dislocation between the source and storage points. Based on experimental observations presented by other authors [21-24], a lower-bound limit of 12 times the burgers

vector has been imposed on $\lambda_{\gamma}^{(\alpha)}$, this accounts for the repulsive force between dislocations and prevents them from becoming infinitely close which would create excessive resistance to deformation. Forest and parallel dislocations are defined as projections of dislocation densities described in ref. [25].
The activation volume is given by

$$V_{c1}^{(\alpha)} = c_{vc1} b^2 \lambda_{\gamma}^{(\alpha)} \tag{10}$$

In order to account for the diffusivity of Re during creep, a dimensionless diffusivity parameter which is a function of temperature and composition has been added to the γ phase flow rule,

$$\Theta(T,\xi) = A(T,\xi)\exp\left(-\frac{Q_o(\xi)}{kT}\right) \tag{11}$$

where ξ denotes the parameter is dependent on composition. The pre-exponential coefficient and the activation energy for diffusion are calculated using Thermo-Calc and DICTRA and experimental creep data. This will be addressed in detail in a later section.
The effective resolved shear stress is calculated as the added contributions of the applied loading, the misfit stresses and the backstress due to the bowing of dislocations:

$$\tau_{eff_{\gamma}}^{(\alpha)} = \tau^{(\alpha)} + \tau_{mis}^{(\alpha)} - \chi^{(\alpha)} \tag{12}$$

The misfit stresses are assumed to relax due to the γ dislocations becoming captured in the γ/γ' interface which causes the loss elastic coherency [19, 20],

$$\tau_{mis}^{(\alpha)}\left(T,\gamma_{\gamma}^{(\alpha)}\right) = \tau_{mis0}^{(\alpha)}\left\{1-\exp\left(\left(\frac{\sum_{\alpha=1}^{12}\rho_{\gamma}^{(\alpha)}}{-\rho_{\gamma}^{ref}}\right)^{c_{icb}}\right)\right\} \tag{13}$$

The backstress is due to the Orowan stress and relates to the bowing of the dislocations in the γ channels between the precipitate interfaces and the forest dislocations and is defined in a similar way as Busso and McClintock [26],

$$\chi^{(\alpha)} = \left(\frac{c_{oro}Gb}{\lambda_{\gamma}^{(\alpha)}} - \tau_{\gamma\ pass}^{(\alpha)}\right) sign\left(\tau_{eff_{\gamma}}^{(\alpha)}\right) \tag{14}$$

The threshold stresses arise from the hardening generated by the passing of dislocations,

$$\kappa_{\gamma}^{(\alpha)} = \tau_{\gamma pass}^{(\alpha)} \tag{15}$$

The passing stress is dependent on the parallel dislocation density within the γ phase (Taylor self-hardening),

$$\tau_{\gamma\ pass}^{(\alpha)} = c_{pass11} Gb\sqrt{\rho_P^{(\alpha)}} \tag{16}$$

In the γ', the flow rule defines the rate of dislocation movement through the γ' precipitates in a ribbon shear fashion on the secondary slip systems,

$$\dot{\gamma}_{L1_2}^{in(\alpha)} = \rho_{L1_2}^{(\alpha)} b \lambda_{L1_2}^{(\alpha)} F_{attack} \exp\left\{\frac{-Q_{slip}^{112} + \left(\left|\tau^{(\alpha)}\right| - \kappa_{L1_2}^{(\alpha)}\right)V_{c2}^{(\alpha)}}{kT}\right\} sign\left(\tau^{(\alpha)}\right) \tag{17}$$

the dislocation mean free path (jump distance) is controlled by the size of the γ′ particles $L_{\gamma'}$ and the interaction with forest dislocations in the γ phase,

$$\lambda_{L1_2}^{(\alpha)} = c_{jump2}\left(\frac{1}{L_{\gamma'}} + \frac{1}{L_{\rho}^{(\alpha)}}\right)^{-1} \tag{18}$$

a lower-bound limit is also imposed on the dislocation spacing of the γ' phase. A close form solution of two strongly-coupled dislocations entering a precipitate is used for this limit [8],

$$\lambda_{\min} = \frac{Gb^2}{\pi\gamma_{APB}} \tag{19}$$

The threshold stresses are a result of the hardening generated by the passing of dislocations and the resistance created from the anti-phase boundary energy,

$$\kappa_{L1_2}^{(\alpha)} = \tau_{L1_2\,pass}^{(\alpha)} + \tau_{APB} \tag{20}$$

The passing stress is defined in a similar way as before,

$$\tau_{L1_2\,pass}^{(\alpha)} = Gbc_{pass22}\sqrt{\rho_P^{(\alpha)}} \tag{21}$$

Finally the anti-phase boundary resistance is described by the anti-phase boundary energy:

$$\tau_{APB} = \frac{\gamma_{APB}}{b} \tag{22}$$

Evolution equations and damage parameter

Internal state variables (ISVs) that evolve with deformation and are tracked on each slip system can be either phenomenological-based [18, 27-31] or dislocation-based [26, 32-34]. Dislocation-based formulations better address the physical process of deformation, though often adding some level of complexity. Additionally, evolution equations may couple mass diffusion/microstructure evolution kinetics to capture microstructural evolution [35-39]. For dislocation-based CVP models, the dislocation density is the primary ISV. The dislocation density in the γ channels, in the γ' particles and in the

γ/γ' interface are controlled by different set of evolution equations since their values are often distinctly different, particularly under conditions when looping of the precipitates occurs, and hence the microstructure attributes that control their evolutions are distinct. In the γ channels, the dislocation density based strain hardening uses the Kocks-Mecking form [40],

$$\dot{\rho}_{\gamma}^{(\alpha)} = \frac{c_{mult1}}{b\lambda_{\gamma}^{(\alpha)}}\left|\dot{\gamma}_{\gamma}^{in(\alpha)}\right| - c_{annh1}\rho_{\gamma}^{(\alpha)}\left|\dot{\gamma}_{\gamma}^{in(\alpha)}\right| \quad (23)$$

This equation assumes evolution depends solely on self-hardening; i.e., hardening depends on the dislocation density on each individual slip system only. The first term represents the multiplication mechanism which is accommodated by additional mobile dislocations with fixed travel distance and the second term represents dynamic recovery associated with the annihilation of parallel dislocations with anti-parallel Burgers vectors within a critical distance.

In the γ' particles, the evolution equation includes one more multiplication term that captures the ease of a dislocations entering the γ' particle, controlled by a thermally activated process

$$\dot{\rho}_{Ll_2}^{(\alpha)} = c_{mult21}\rho_{pb}^{(\alpha)}\Gamma + \frac{c_{mult22}}{b\lambda_{\gamma'}^{(\alpha)}}\left|\dot{\gamma}_{\gamma'}^{(\alpha)}\right| - c_{annh2}\rho_{\gamma'}^{(\alpha)}\left|\dot{\gamma}_{\gamma'}^{(\alpha)}\right| \quad (24)$$

where,

$$\begin{cases} \Gamma = F_{attack}\exp\left\{\dfrac{-Q_{\text{climb}}^{pb} + \left(\left|\tau^{(\alpha)}\right| - \tau_{pb_{pass}}^{(\alpha)}\right)V_{c2}^{(\alpha)}}{kT}\right\} \\ Q_{\text{climb}}^{pb} = c_{misfit}Gb^3\left|\delta\right| \\ \tau_{pb_{pass}}^{(\alpha)} = c_{pass21}Gb\sqrt{\rho_{P_{pb}}^{(\alpha)}} \end{cases} \quad (25)$$

The first term of equation (24) considers the contribution from the dislocations that are generated in the channels and then gather at the phase boundary (γ/γ' interface). Enough dislocations need to gather at the interface to start cutting the precipitates. The formation of these dislocations increases the incoherency of the precipitates making them harder to be cut, this is accounted for using by the interface passing stress and is a function of parallel dislocation density at the γ/γ' interface.

The evolution equations for dislocations gathered at the interface also uses the Kocks-Mecking form and is dependent on the shearing rates in the γ channels:

$$\dot{\rho}_{pb}^{(\alpha)} = \frac{c_{mult}^{pb}}{bL_{\gamma}}\left|\dot{\gamma}_{\gamma}^{in(\alpha)}\right| - c_{annh}^{pb}\rho_{pb}^{(\alpha)}\left|\dot{\gamma}_{\gamma}^{in(\alpha)}\right| \quad (26)$$

Damage is accounted for through the void condensation generated by the annihilation of dislocations in the γ phase, the γ' phase and in the γ/γ' interface. It is assumed that a single vacancy is b^3 in volume, and that the evolution equations for the radius of the voids are proportional to the annihilation terms in the evolution of the dislocation densities:

$$\begin{cases} \dot{R}_{\gamma}^{(\alpha)} = c_{void11}\dfrac{c_{annh1}\rho_{\gamma}^{(\alpha)}\left|\dot{\gamma}_{\gamma}^{in(\alpha)}\right|b^2}{2} \\ \dot{R}_{pb}^{(\alpha)} = c_{void12}\dfrac{c_{annh1}\rho_{pb}^{(\alpha)}\left|\dot{\gamma}_{\gamma}^{in(\alpha)}\right|b^2}{2} \\ \dot{R}_{\gamma'}^{(\alpha)} = c_{void22}\dfrac{c_{annh2}\rho_{\gamma'}^{(\alpha)}\left|\dot{\gamma}_{\gamma'}^{in(\alpha)}\right|b^2}{2} \end{cases} \quad (27)$$

the damage parameter at a time t is calculated by considering the contributions of all the voids that form in the γ phase, the γ' phase and in the γ/γ' interface

$$D = \left(\int_{t=0}^{t=t}\left(\sum_{\alpha=1}^{12}\dot{R}_{\gamma}^{(\alpha)} + \sum_{\alpha=1}^{12}\dot{R}_{pb}^{(\alpha)} + \sum_{\alpha=13}^{24}\dot{R}_{\gamma'}^{(\alpha)}\right)d\tau\right)^{\frac{2}{3}} \quad (28)$$

the exponent 2/3 converts the volume ratio to the effective cross-sectional area of shearing. Finally the effective applied resolved shear stress becomes:

$$\tau^{(\alpha)} = \frac{\tau_{applied}^{(\alpha)}}{1-D} \quad (29)$$

Composition sensitive diffusivity term in flow rule

In hot section industrial gas turbine components that operate at high temperatures, diffusion of atoms, which is a thermally-induced phenomenon, is a significant factor in controlling the creep response of the material. Primary creep is a combination of dislocation glide and climb in γ channels and at γ/γ´ interfaces. Climb of dislocations is a diffusion-controlled and therefore thermally activated mechanism necessary for dislocations to proceed gliding in channels. Additionally, during tertiary creep, once the $a<11\bar{2}>$ dislocation ribbons are formed by dissociation into Shockley partials, it is likely that shearing of the γ´ precipitates is controlled by diffusion due to the atomic adjustments required at the onset of dislocation movements at γ´ phase [41, 42]. As was previously discussed, rafting of the microstructure also involves interdiffusion of the atoms between the vertical and horizontal channels. Therefore, introducing a diffusivity parameter in the flow rule of γ channel provides the means to rigorously describe and capture physics of creep. The diffusivity parameter is defined by equation(11). To determine this parameter and incorporate it in the flow rule, a study on effective diffusivity of the system is conducted by means of kinetic software DICTRA interfaced with thermodynamic software Thermo-Calc [43] which performs all the required thermodynamic calculations.

Estimation of effective diffusivity with DICTRA

DICTRA is a software for simulation of diffusion-controlled processes such as homogenization of alloys, micro-segregation during solidification, and coarsening of precipitates in multicomponent alloys through solving Fick-Onsager law [44, 45]

$$\tilde{J}_i = -\sum_{j=1}^{n-1} \tilde{D}_{ij} \frac{\partial c_j}{\partial z} \tag{30}$$

where $\tilde{J}_i$ is the atomic flux and $\tilde{D}_{ij}$ is $(n\text{-}1)^2$ temperature and composition dependent diffusivity matrix.

The simulations are based on assessed thermodynamic and mobility databases that have been developed using CALPHAD method [46]. The accuracy of the simulations strongly depends on the quality of these databases. In present work TCNi5 [47] thermodynamic and MOBNi2 [48] mobility databases have been used to determine the composition-sensitive effective diffusivity.

The equation to describe the effective diffusivity, as is expected, exhibits an Arrhenius form [49],

$$D_{eff} = D_{0,eff} exp\left(-\frac{Q_{eff}}{kT}\right) \tag{31}$$

where Q_{eff} and $D_{0,eff}$ are the activation energy and pre-exponential factor for effective diffusion coefficient, respectively, and can be described by arithmetic and harmonic mean equations such that composition sensitivity is captured and the contribution of each element to the effective values is balanced by their atomic concentration, C_m [50],

$$Q_{eff} = \sum_m C_m Q_{Ni-m} \tag{32}$$

$$D_{0,eff} = \frac{1}{\sum_m \frac{C_m}{D_{0,Ni-m}}} \tag{33}$$

in these equations, Q_{Ni-m} and $D_{0,Ni-m}$ are the activation energy and the pre-exponential factor of element *m* and Ni interdiffusion coefficient (chemical diffusivity), respectively.

Diffusivity paths are essentially created in γ channels. Moreover, vacancy exchange and dislocation climb during rafting and creep takes place in the disordered γ phase. Hence, effective diffusivity of the material is equivalent to the effective diffusivity in γ channels.

In order to estimate the composition sensitivity of introduced parameters and evaluate the influence of Re content variation, three compositions with different Re contents (0% Re, 3% Re and 6% Re) were defined in addition to CMSX-8 (1.5%Re). Calculations on composition segregation in γ and γ′ phases were carried out at 1000°C for each system in DICTRA. Chemical compositions of the γ channels for each unique system are presented in

Table II. The results enabled defining of the binary Ni-m couple based on the corresponding composition of element m in γ phase.

Interdiffusion coefficients of the binary systems were obtained from the MOBNi2 mobility database in the temperature range of 700°C to 1100°C using the equilibrium compositions (

Table II). By fitting the chemical diffusivity values to an Arrhenius type relation as a function of temperature, desired diffusion parameters including Q_{Ni-m} and $D_{0,Ni-m}$ were acquired for all binary systems. The effective diffusivity parameter of Eq. (30) for different Re content compositions were estimated using Eq. (31) and (32). The calculated values are tabulated in Table III.

This method has shown to have good agreement with experimental results. For CMSX-4®, the calculated value of Q_{eff} is 271.7 *kJ/mol* compared to the experimentally measured value of 272.4 *kJ/mol* [50].

Table II. Equilibrium composition in wt. % of the γ phase at 1000°C (balance Ni).

	0% Re	1.5% Re	3% Re	6% Re
Cr	10.0	10.0	10.3	10.7
Co	18.6	19.0	19.4	20.0
Mo	1.1	1.2	1.2	1.3
W	15.0	15.4	15.8	16.6
Al	2.8	2.5	2.2	1.7
Ti	0.3	0.2	0.19	0.1
Ta	1.9	1.5	1.2	0.7
Re	0.0	3.2	606	13.7
Hf	0.02	0.02	0.02	0.01

Figure 5 illustrates effective diffusivity versus temperature for compositions with distinct Re content following equation (30). It is observed that increase in the refractory element Re is accompanied by a reduction in the effective diffusivity and temperature sensitivity of the material.

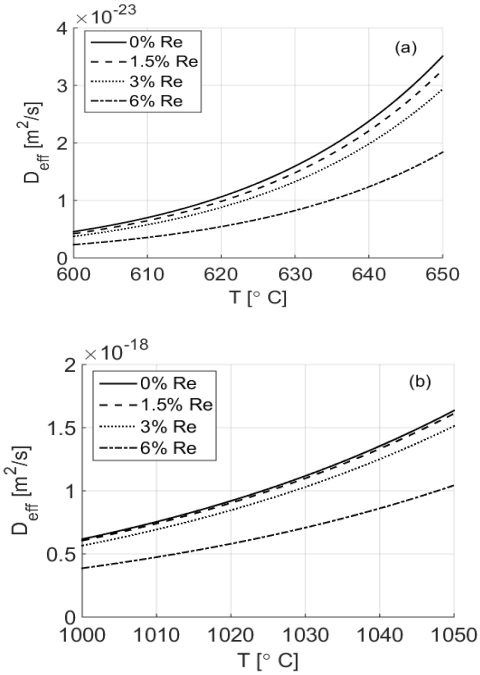

Figure 5. Effective diffusivity versus temperature illustrating the effect of various Re content in temperature range (a) 600-650ºC (b) 1000-1050ºC.

It is evident from these plots that sensitivity to composition is not linear such that the influence of Re addition is considerably more effective from 3% to 6% than it is from 0% to 3%. As the temperature increases, this effect becomes more pronounced in such a way that by introducing a small amount of Re to the system, a slight decrement of effective diffusivity is observed whereas with higher Re content, diffusion has been decelerated extensively (Figure 5(b)).

Table III. Effective diffusivity parameters for four composition combinations.

	0% Re	1.5% Re	3% Re	6% Re
Q_{eff} (kJ/mol)	272.9	274.7	275.4	277.8
$D_{0,eff}$ (m^2/s)	9.69E-8	1.09E-7	1.13E-7	9.73E-8

So far, the effective diffusivity of CMSX-8 has been characterized as a function of composition and temperature. Thereafter, effective terms can be incorporated in the diffusivity parameter of equation (7) resulting in a composition and temperature sensitive flow rule. The constitutive model was calibrated against experimental results with effective activation energy being substituted as $Q_0(\xi)$ in equation (11). By calibrating the model to available experimental data, the pre-exponential factor $A(T,\xi)$ was found to be a function of temperature; conceptually it could also be a function of the composition of the alloy using this coefficient.

Model predictions

The model material parameters were calibrated from creep response data at temperatures ranging from 750 to 1037ºC and stresses ranging from 124 to 700 MPa. This range of test conditions allows for the model be calibrated for both primary and tertiary deformation regimes.

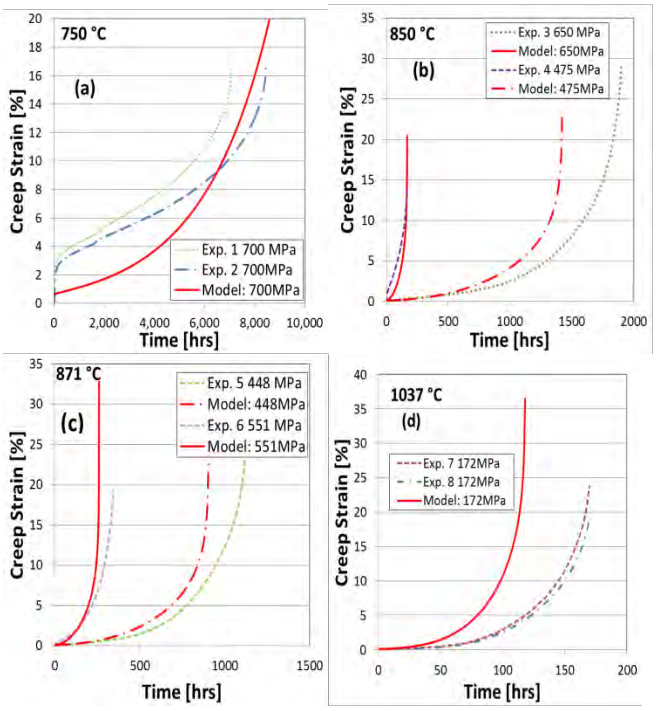

Figure 6. Creep response under for different loading conditions

As shown in Figure 6, the model readily captures all regimes of creep for CMSX-8. In Figure 6 (a) it accurately predicts that the deformation will show significant primary creep; which is in agreement with data from Figure 4. At this higher stress level there is enough force for dislocations to cut through the γ' precipitates thus promoting primary creep. Furthermore note that in Figure 6 (b) and Figure 6 (c) the deformation shows some primary creep but is largely dominated by tertiary creep also consistent with Figure 4. At the highest temperature 1037ºC, there is no visible primary creep and the deformation is completely dominated by tertiary creep as seen in Figure 6 (d). The model parameters constants used in this work are given in Table IV and Table V.

A novel feature of this model is the incorporation of a composition sensitive diffusivity parameter. The form of $A(T,\xi)$ in Eq.(11) is assumed to have a power law,

$$A(T,\xi) = C_1(\xi)\left(\frac{T}{T_{melt}}\right)^{C_2} \tag{34}$$

where T is given in degrees Kelvin and ξ is used to indicate that the parameter is a function of the composition of the alloy. $C_1(\xi)$ and C_2 were found to be $1.59\text{x}10^8$ and -23, respectively.

Table IV. Fundamental microstructure parameters

Fundamental parameters		Microstructure parameters	
b	2.49 (Å)	Virgin microstructure:	
F_{attack}	$1x10^{12}$ [1/s]	f_γ	0.3
γ_{APB}	0.111 [J/m^2]	$f_{\gamma'}$	0.7
δ	-0.002	L_γ	$0.14x10^{-6}$ [m]
T_{melt}	1726 [K]	$L_{\gamma'}$	$0.74x10^{-6}$ [m]

Table V. Parameters fitted to creep deformation data

c_{annh1}	10.0	c_{pass11}	0.22
c_{annh}^{pbd}	10.0	c_{pass22}	1.20
c_{annh2}	5.0	c_{pass21}	0.15
c_{Fdis}	10.0	c_{vc1}	1.0
c^{icb}	5.0	c_{vc2}	$8.4\text{x}10^{-1}$
c_{jump1}	$6\text{x}10^{-2}$	c_{void11}	$8\text{x}10^3$
c_{jump2}	$6\text{x}10^{-2}$	c_{void22}	$1\text{x}10^3$
c_{misfit}	180 [1/mol]	c_{void21}	$8\text{x}10^3$
c_{mult1}	$3\text{x}10^{-3}$	Q_{slip}^{110}	360 [kJ/mol]
c_{mult}^{pbd}	$1\text{x}10^{-3}$	Q_{slip}^{112}	105 [kJ/mol]
c_{mult2}	$9.3\text{x}10^{-4}$	$\rho_\gamma^{(\alpha)}\|_{t=0}$	$1\text{x}10^{11}$ [1/m^2]
c_{mult21}	$5\text{x}10^{-16}$	$\rho_{\gamma'}^{(\alpha)}\|_{t=0}$	0 [1/m^2]
c_{oro}	$2.2\text{x}10^{-2}$	ρ_γ^{ref}	$1.0\ \text{x}10^{13}$

Rafting of the microstructure was not considered in this model. In the aging studies, rafting became observable for temperatures of 950 ºC and above. Rafting plays a role in the response of creep and more research is needed to incorporate it in the model. Modeling of the evolution of the microstructure during rafting is necessary to completely account for the deformation of CMSX-8. This could be accomplished by utilizing equation (3) as an evolution equation for the morphology of the microstructure and then modifying the model to consider a parameter that instead of assuming a cuboidal microstructure, where the hardening can be described exclusively by the length of the precipitates, it utilizes a more elaborate formulation where the aspect ratio the precipitates in the evolved microstructure is considered instead, as done in reference [5].

Conclusions and future work

We presented three different tools that can enable the ICME of Ni-base superalloys. In the first tool equations that can predict the microstructure evolution during aging were developed, these equations can be used to determine the geometry of the

microstructure which can serve as an input in CVP models. In the second tool a composition sensitive CVP model is developed that can consider the Re content in the alloy and is capable of predicting the creep behavior of CMSX-8. In the final tool, computational kinetics modeling is used to determine the value of composition-sensitive parameters in the CVP model. Although still in its infancy, the integration and further development of the tools presented can help pave the way for alloy design and design of components with controlled spatial microstructure variations. In future work the aging equations will be used in the CVP to explicitly model the rafting regime in this alloy.

Acknowledgments

This work is supported by U.S. Department of Energy, National Energy Technology Laboratory, University Turbine Systems Research (UTSR) Program, Grant DE-FE0011722, and Siemens Energy Inc., Orlando, FL.

References

1. Wahl, J. B. and K. Harris. *New Single Crystal Superalloys, CMSX-7 and CMSX-8*. in *Superalloys 2012* Seven Springs Mountain Resort,Seven Springs, PA: TMS.

2. Harris, K., et al., *Development of the rhenium containing superalloys CMSX-4 and CM 186 LC for single crystal blade and directionally solidified vane applications in advanced turbine engines*, in *Superalloys 1992*, R. W. Stusrud S. D. Antolovich, R. A. MacKay, D. L. Anton, T. Khan, R. D. Kissinger, D. L. Klarstrom, Editor. 1992, The Minerals, Metals and Materials Society (TMS): Warrendale, PA. p. 297-306.

3. Wahl, J. B. and K. Harris, *NEW SINGLE CRYSTAL SUPERALLOYS, CMSX (R)-7 AND CMSX (R)-8.* Superalloys 2012, 2012: p. 179-188.

4. Fullwood, D. T., S. R. Niezgoda and S. R. Kalidindi, *Microstructure reconstructions from 2-point statistics using phase-recovery algorithms.* Acta Materialia, 2008. **56**(5): p. 942-948.

5. Kirka, Michael, *Thermomechanical behavior of a directionally solidified nickel-base superalloy in the aged state*, in *The George W. Woodruff School of Mechanical Engineering*. 2014, Georgia Institute of Technology: Atlanta, Georgia p. 230.

6. Jaroszewicz, J., et al., *Characterization of Single-Crystal Dendrite Structure and Porosity in Nickel-Based Superalloys Using X-Ray Micro-Computed Tomography.* Euro Superalloys 2010, 2011. **278**: p. 66-71.

7. Epishin, A., et al., *Effects of segregation in nickel-base superalloys: Dendritic stresses.* Superalloys 2004, 2004: p. 537-543.

8. Reed, Roger C., *Superalloys - Fundamentals and Applications*. 2006: Cambridge University Press.

9. Epishin, A., et al., *Microstructural degradation of CMSX-4: Kinetics and effect on mechanical properties.* Superalloys 2008, 2008: p. 725-731.

10. Reed, R. C., *The superalloys fundamentals and applications*. 1st ed. 2006: Cambridge University press.

11. Fullwood, D. T., et al., *Microstructure sensitive design for performance optimization.* Progress in Materials Science, 2010. **55**(6): p. 477-562.

12. Nabarro, F. R. N., *Rafting in superalloys.* Metallurgical and Materials Transactions a-Physical Metallurgy and Materials Science, 1996. **27**(3): p. 513-530.

13. Tinga, T., W. A. M. Brekelmans and M. G. D. Geers, *Directional coarsening in nickel-base superalloys and its effect on the mechanical properties.* Computational Materials Science, 2009. **47**(2): p. 471-481.

14. Matan, N., et al., *On the kinetics of rafting in CMSX-4 superalloy single crystals.* Acta Materialia, 1999. **47**(7): p. 2031-2045.

15. Mushongera, L. T., et al., *Effect of Re on directional gamma '-coarsening in commercial single crystal Ni-base superalloys: A phase field study.* Acta Materialia, 2015. **93**: p. 60-72.

16. Asaro, R. J., *Crystal Plasticity.* Journal of Applied Mechanics-Transactions of the Asme, 1983. **50**(4B): p. 921-934.

17. Tinga, Tiedo, W. A. Brekelmans and Marc G. D. Geers, *Cube slip and non-Schmid effects in single crystal Ni-base superalloys.* Modeling and simulation in material science and engineering 2010. **18**.

18. Staroselsky, A. and B. N. Cassenti, *Creep, plasticity, and fatigue of single crystal superalloy.* International Journal of Solids and Structures. **48**: p. 2060-2075.

19. Ma, A., D. Dye and R. C. Reed, *A model for the creep deformation behaviour of single-crystal superalloy CMSX-4.* Acta Materialia, 2008. **56**(8): p. 1657-1670.

20. Pollock, T. M. and A. S. Argon, *Creep Resistance of CMSX-3 Nickel-Base Superalloy Single-Crystals.* Acta Metallurgica Et Materialia, 1992. **40**(1): p. 1-30.

21. Pollock, T. M. and A. S. Argon, *Creep resistance of CMSX-3 nickel base superalloy single crystals.* Acta Metallurgica et Materialia, 1992. **40**(1): p. 1-30.

22. Rae, C., et al., *Dislocations in a Ni-based superalloy during low temperature creep.* Eurosuperalloys 2014 - 2nd European Symposium on Superalloys and Their Applications, 2014. **14**.

23. Zhang, J. X., et al., *Creep deformation mechanisms in some modern single-crystal superalloys.* Superalloys 2004, 2004: p. 189-195.

24. Koizumi, Yutaka, et al., *Development of next-generation Ni-base single cyrstal superalloys.* Superalloys 2004, 2004: p. 35-43.

25. Ma, A. and F. Roters, *A constitutive model for fcc single crystals based on dislocation densities and its application to uniaxial compression of aluminium single crystals.* Acta Materialia, 2004. **52**(12): p. 3603-3612.

26. Busso, E. P. and F. A. McClintock, *A dislocation mechanics-based crystallographic model of a B2-type intermetallic alloy.* International Journal of Plasticity, 1996. **12**(1): p. 1-28.

27. Österle, W., et al., *Modelling the orientation and direction dependence of the critical resolved shear stress of nickel-base superalloy single crystals.* Acta Materialia, 2000. **48**(3): p. 689-700.

28. Sheh, M. Y. and D. C. Stouffer, *A Crystallographic Model for the Tensile and Fatigue Response for Rene N4 at 982°C.* Journal of Applied Mechanics, 1990. **57**(1): p. 25-31.

29. Meric, L., P. Poubanne and G. Cailletaud, *Single Crystal Modeling for Structural Calculations: Part 1 - Model Presentation.* Journal of Engineering Materials and Technology, 1991. **113**: p. 162-170.

30. Meric, L. and G. Cailletaud, *Single Crystal Modeling for Structural Calculations: Part 2 - Finite Element Implementation.* Journal of Engineering Materials and Technology, 1991. **113**: p. 171-182.

31. Shenoy, M. M., et al., *Thermomechanical fatigue behavior of a directionally solidified Ni-base superalloy.* Journal of Engineering Materials and Technology-Transactions of the Asme, 2005. **127**(3): p. 325-336.

32. Song, J. E. and D. L. McDowell, *Grain Scale Crystal Plasticity Model with Slip and Microtwinning for a Third Generation Ni-Base Disk Alloy.* Superalloys 2012, 2012: p. 159-166.

33. Shenoy, Mahesh, Yustianto Tjiptowidjojo and David McDowell, *Microstructure-sensitive modeling of polycrystalline IN 100.* International Journal of Plasticity, 2008. **24**(10): p. 1694-1730.

34. Wang, A. J., et al., *Microstructure-based multiscale constitutive modeling of gamma-gamma ' nickel-base superalloys.* International Journal for Multiscale Computational Engineering, 2006. **4**(5-6): p. 663-692.

35. Zhao, L. G., N. P. O'Dowd and E. P. Busso, *A coupled kinetic-constitutive approach to the study of high temperature crack initiation in single crystal nickel-base superalloys.* Journal of the Mechanics and Physics of Solids, 2006. **54**(2): p. 288-309.

36. Dumoulin, S., et al., *A multiscale approach for coupled phenomena in fcc materials at high temperatures.* Philosophical Magazine, 2003. **83**(31-34): p. 3895-3916.

37. Fedelich, B., et al., *Constitutive modelling of creep degradation due to rafting in single-crystalline Ni-base superalloys.* Materials Science and Engineering a-Structural Materials Properties Microstructure and Processing, 2009. **510-11**: p. 273-277.

38. Fedelich, B., et al., *Rafting during High Temperature Deformation in a Single Crystal Superalloy: Experiments and Modeling.* Superalloys 2012, 2012: p. 491-500.

39. Basoalto, H., et al., *A generic microstructure-explicit model of creep in nickel-base superalloys.* Superalloys 2004, 2004: p. 897-906.

40. Kocks, U. F. and H. Mecking, *Physics and phenomenology of strain hardening: the FCC case.* Progress in Materials Science, 2003. **48**(3): p. 171-273.

41. Rae, C. M. F. and R. C. Reed, *Primary creep in single crystal superalloys: Origins, mechanisms and effects.* Acta Materialia, 2007. **55**(3): p. 1067-1081.

42. Yang, H., M. S. Huang and Z. H. Li, *The influence of vacancies diffusion-induced dislocation climb on the creep and plasticity behaviors of nickel-based single crystal superalloy.* Computational Materials Science, 2015. **99**: p. 348-360.

43. Andersson, J. O., et al., *THERMO-CALC & DICTRA, computational tools for materials science.* Calphad-Computer Coupling of Phase Diagrams and Thermochemistry, 2002. **26**(2): p. 273-312.

44. Borgenstam, A., et al., *DICTRA, a tool for simulation of diffusional transformations in alloys.* Journal of Phase Equilibria, 2000. **21**(3): p. 269-280.

45. Wang, C. P., et al., *Diffusion mobilities in the fcc Ag-Cu and Ag-Pd alloys.* Calphad-Computer Coupling of Phase Diagrams and Thermochemistry, 2012. **37**: p. 57-64.

46. Agren, J., *Calculation of phase diagrams: Calphad.* Current Opinion in Solid State & Materials Science, 1996. **1**(3): p. 355-360.

47. McDowell, David L., *Viscoplasticity of heterogeneous metallic materials.* Materials Science and Engineering: R: Reports, 2008. **62**(3): p. 67-123.

48. Giordana, M. F., et al., *Micromechanical modeling of the cyclic softening of EUROFER 97 steel.* Procedia Engineering, 2011. **10**: p. 1268-1273.

49. Zhu, Z., et al., *A model for the creep deformation behaviour of nickel-based single crystal superalloys.* Acta Materialia, 2012. **60**(12): p. 4888-4900.

50. Ai, C., et al., *Application of a modified Ostwald ripening theory in coarsening of gamma ' phases in Ni based single crystal superalloys.* J. of Alloys and Compounds, 2015. **632**: p. 558-562.